# Mean field representation of the natural and actuated cylinder wake

Gilead Tadmor,[1,a)] Oliver Lehmann,[2] Bernd R. Noack,[3] and Marek Morzyński[4]
[1]*Department of Electrical and Computer Engineering, Northeastern University, 440 Dana Research Building, Boston, Massachusetts 02115, USA*
[2]*Department of Fluid Dynamics and Engineering Acoustics, Berlin Institute of Technology MB1, Straße des 17. Juni 135, D-10623 Berlin, Germany*
[3]*Institut Pprime, CNRS—Université de Poitiers—ENSMA, UPR 3346, Département Fluides, Thermique, Combustion, CEAT, 43 rue de l'Aérodrome, F-86036 Poitiers Cedex, France*
[4]*Institute of Combustion Engines and Transportation, Poznań University of Technology, ul. Piotrowo 3, PL-60-965 Poznań, Poland*

(Received 1 April 2009; accepted 22 September 2009; published online 12 March 2010)

The necessity to include dynamic mean field representations in low order Galerkin models, and the role and form of such representations, are explored along natural and forced transients of the cylinder wake flow. The shift mode was introduced by Noack *et al.* [J. Fluid Mech. **497**, 335 (2003)] as a least-order Galerkin representation of mean flow variations. The need to include the shift mode was argued in that paper in terms of the dynamic properties of a low order Galerkin model. The present study revisits and elucidates this issue with a direct focus on the Navier–Stokes equations (NSEs) and on the bilateral coupling between variations in the fluctuation growth rate and mean flow variations in the NSE. A detailed transient modal energy flow analysis is introduced as a new tool to quantitatively demonstrate the indispensable role of mean field variations, as well as the capacity of the shift mode to represent that contribution. Four variants of local and global shift mode derivations are examined and compared, including the geometric approach of Noack *et al.* and shift modes derived by a direct appeal to the NSE. Combined with the conclusions of the energy flow analysis, the similarity of the resulting shift modes indicates that the shift mode is no accident: indeed it is an intrinsic component of transient dynamics. Mean field representations can be found as implicit components in successful low order Galerkin models. We therefore argue for the benefit of the simple and robust explicit formulation in terms of added shift modes. © *2010 American Institute of Physics*. [doi:10.1063/1.3298960]

## I. INTRODUCTION

Very low order Galerkin models are typically based on modes representing the dominant instability in the flow. By this standard practice, models may use empirical Karhunen–Loève/proper orthogonal decomposition (POD) of an attractor,[1–7] employ linear stability eigenmodes,[8–11] or, more recently, be derived by linear-operator-theoretic model reduction methods, such as the balanced POD.[12–15] While an efficient kinematic approximation of dominant coherent structures may be feasible with very few modes, all too often the corresponding Galerkin model is incapable to properly predict the dynamic behavior,[16,17] to the point that stability properties of solutions of the Navier–Stokes equation (NSE) may be reversed in the reduced order system.[18,19] In contrast, an effective model should capture dynamics not only over the attractor limit cycle, but also over the corresponding attractive inertial manifold[20] that connects the unstable fixed point with the limit cycle. This paper highlights the absence of adequate mean field representations, as one cause for such difficulties, and investigates means to incorporate mean field dynamics in low order Galerkin models, as a remedy.

Consider laminar two-dimensional (2D) wake flows as an illustration. Whereas a single POD mode pair provides an excellent attractor resolution, the associated Galerkin model is of no dynamic value:[17] the marginally stable Galerkin (oscillator) model is structurally unstable and incapable of predicting even the attractor's energy level, let alone growth rates. An increase in the number of POD modes[16] may offer only a partial improvement.[17] Even the balanced POD approach, with its direct focus on dynamics, fails by predicting a global instability in systems dominated by an unsteady attractor.[21] This deficiency is detrimental to the use of reduced order Galerkin models as efficient encapsulations of dominant flow physics features, and in some cases, to their use in feedback control design, where both transient representation capabilities and very low dimension may be essential.

As shown in Ref. 17, a key deficiency of both standard POD models and of linearization-based models is the exclusion of the interaction of oscillatory unsteadiness with the mean flow. From the perspective elaborated in Ref. 17, what is missing is a representation of the state-space direction of the transient mean field correction. That direction is excluded in attractor-focused POD bases. It eludes linear stability analysis and (linear) balanced POD constructions, due the intrinsic nonlinearity of the interactions of unsteady fluctuations with the mean field.

These observations connect with the seminal work on

a)Electronic mail: tadmor@coe.neu.edu.

 

POD representations of the turbulent boundary layer in Ref. 22 and are at the foundation of mean field theory, introduced in Refs. 23 and 24 and continued in Refs. 25–28. The *shift mode* was introduced in Refs. 17 and 29 as a POD model augmentation that represents the nonlinear dynamic effects of mean field corrections and a key enabler for the dynamic representation of transients. In the cylinder wake flow example, augmentation by a single shift mode transforms an unusable model into a robust representation of the system's key dynamic properties. Similar and related observations and applications to feedback flow control were made by the present authors and by others in a variety of contexts and configurations.[17,23–25,28–37] Investigation of the dynamic role of *nonlinear mean field corrections* in flow control where carried also by Wesfreid, Protas, and collaborators, e.g., in Refs. 38–40.

The need for a mean field model was explained in Ref. 17 in terms of the feasible dynamic envelope of a least-order Galerkin system. In this sense, it provides a global extension of Landau's amplitude equation.[41–43] The objective of the current presentation is to explore a complementary perspective, based on a direct appeal to the NSE: building on the seminal ideas of Ref. 22, the NSE is partitioned as a system coupling the Reynolds averaged NSE (RANSE) and a band-pass filtered variant. The need for a mean field model and its ideal, local form, are now derived from the dynamically essential bilateral coupling between variations in the fluctuation growth rate and variations in the mean field. Standard POD models represent only the band-pass filtered NSE and therefore cannot properly adjust the fluctuation growth rates along transients. The mean field model remedies this deficiency, serving as a complementary, Galerkin–Reynolds equation, representing the NSE mechanism to adjust fluctuation growth rates.

Modal energy flow analysis of transient dynamics is introduced as a new tool, quantifying the instantaneous dynamic role of individual flow components. Here, it is used to demonstrate how excluding mean field variation may lead to dramatic distortions, ranging from global exponential growth to the elimination of the instability near the steady solution. In contrast, including a crude representation of mean field variations by a single shift mode, suffices for a decent dynamic approximation of the exact NSE solution, even with the simplest, least-order approximation of the unsteady fluctuations by a single POD mode pair.

The paper further aims to establish connections between the dynamic-analytic perspective on mean field models and easily computed, empirical-kinematic representations. Global and local dynamic definitions of the shift mode will thus be compared with kinematic counterparts, based on the extraction of the orientation of base flow changes from natural and actuated transient data. These approaches will be examined and compared using the natural and actuated laminar 2D wake flow behind a circular cylinder as a benchmark. The results reveal both a fundamental consistency, and points of departure, such as due to the contribution of periodic actuation to the Reynolds stress. The similarity of alternative shift mode definitions and the sufficiency of the simplest definition, as noted above, therefore complement the dual message

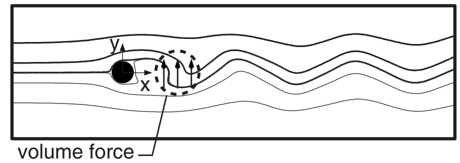


FIG. 1. The actuated cylinder wake: the cylinder is represented by the black disk. The downstream circle and arrows indicate the location and orientation of a volume-force actuator. Streamlines represent a snapshot of the natural flow. Thick (thin) curves correspond to positive (negative) values of the stream-function—here and in all following flow visualizations.

of this paper, that mean field variations can often be amply resolved by very simple means.

The paper is organized as follows: a brief review of the cylinder wake benchmark is provided in Sec. II. Mean field theory is discussed in Sec. III, including motivation and background, the NSE-based analytic framework, and a quantitative demonstration in terms of transient modal energy flow analysis. Candidate shift mode definitions are stated and discussed in Sec. IV and compared quantitatively in Sec. V. Concluding remarks are brought in Sec. VI. The Appendix elucidates the control aspects of the forced trajectories, which are secondary to the paper's focus.

## II. THE CYLINDER WAKE BENCHMARK

The cylinder wake flow serves as an illustration and a test-case for validation of the concepts presented in this paper. The key characteristics are reviewed in Sec. II A, followed by Sec. II B with details of the simulations data used. The concept and computation of a flow representation with a dynamic base flow are discussed in Sec. II C.

### A. The laminar 2D cylinder wake flow

Figure 1 depicts the cylinder wake configuration. The Cartesian coordinates, $x$ and $y$, are aligned with the incoming flow and transverse direction. Boldface is used for an abbreviated vector notation [e.g., $\mathbf{x}=(x,y)$]. The cylinder, represented by the black disk, occupies the area

$$\Omega_D = \{\mathbf{x} \in \mathcal{R}^2 : \|\mathbf{x}\| \leq 1/2\},$$

where we relate to the Euclidean norm $\| \, \|$. The flow is represented by streamlines over a subset of the computational domain

$$\Omega = \{\mathbf{x} \in \mathcal{R}^2 \setminus \Omega_D : x \in [-5,15], y \in [-5,5]\}.$$

The velocity field is $\mathbf{u}=(u,v)$, where the components $u$ and $v$ are, respectively, aligned with the $x$ and $y$ axes.

Figure 1 also includes a vertical volume force, defined over the domain indicated by the downstream disk

$$\mathbf{f}(\mathbf{x},t) = G(t)\mathbf{g}(\mathbf{x}), \quad \text{where}$$

$$\mathbf{g}(\mathbf{x}) = \begin{cases} (0,1), & \mathbf{x} \in \Omega_G, \\ (0,0), & \text{otherwise}, \end{cases} \tag{1}$$

$$\Omega_G = \{\mathbf{x} \in \mathcal{R}^2 : \|\mathbf{x} - (0,2)\| \leq 1\}.$$

The modulating amplitude $G(t)$ is viewed here as a control command whose purpose is discussed in Sec. II B below.

The flow is characterized by the Reynolds number

$$\mathrm{Re} = \frac{U_\infty D}{\nu},$$

where $U_\infty$ is the velocity of the oncoming flow, $D$ is the diameter of the cylinder, and $\nu$ is the kinematic viscosity of the fluid. In the sequel, all quantities are nondimensionalized with respect to the cylinder diameter $D$, the flow velocity $U_\infty$, and the fluid density $\rho$.

The incompressible flow satisfies the continuity equation

$$\nabla \cdot \mathbf{u} = 0, \tag{2a}$$

and the NSE

$$\partial_t \mathbf{u} + \nabla \cdot (\mathbf{u} \otimes \mathbf{u}) + \nabla p - \frac{1}{\mathrm{Re}} \Delta \mathbf{u} - \mathbf{f} = 0, \tag{2b}$$

where the control term $\mathbf{f}$ represents the actuation volume force in Fig. 1, as defined in Eq. (1). The empirical data used in this paper was produced by direct numerical simulations (DNS) of the incompressible NSE (2) on a symmetric grid with 8712 nodes distributed over the specified domain.

The wake flow becomes unstable at $\mathrm{Re} \approx 47$.[8,44] The simulation data used in our presentation were obtained at $\mathrm{Re}=100$, i.e., far above this onset value and far below the transition Reynolds number of 180, where three-dimensional instabilities become important.[45–48] At this Reynolds number, the natural flow converges to a periodic state associated with von Kármán vortex shedding. This periodic solution is strongly dominated by the first temporal harmonic at the shedding frequency. The first POD mode pair reflects this first shedding harmonic and resolves some 95% of the fluctuation energy.[16] Similarly, the early transient, initiated by a small perturbation of the unstable, steady solution, is dominated by the two eigenmodes, associated with the instability. Furthermore, fluctuations of each single period of the natural transient from the time-windowed averages are dominated by a single pair of coherent flow structures, which continuously morph from the instability eigenmodes to the dominant attractor POD modes.[34,35,49]

### B. Simulation data

Two simulation trajectories will be used as empirical data in quantitative analysis. Figures 2 and 3 represent these trajectories by the respective phase-averaged fluctuation energy, $\mathcal{K}$, termed hereafter the *turbulent kinetic energy*, and by the actuation level. The computation of $\mathcal{K}$ is deferred to Sec. II C.

The natural transient from a small perturbation of the unstable steady NSE solution to the attractor, depicted in Fig.

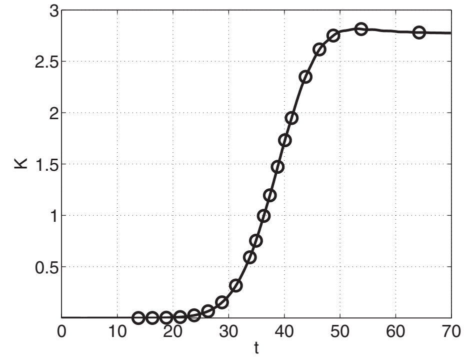


FIG. 2. The time evolution of the fluctuation energy, $\mathcal{K}$, of the natural transient from the steady solution to the attractor. Circles along the curve mark the midpoints of 20 single-period (and partially overlapping) time intervals that are used to obtain local shift modes.

2, represent the inertial manifold[20] and is a simple but generic example of unforced flow behavior in systems with an unsteady attractor. This trajectory will be referred to, thenceforth, as the *natural transient* (i.e., suppressing mention of its beginning and end). A moderately actuated transient, in Fig. 3, is a generic example of feedback controlled flow transients. A common flow control objective is to suppress vortex shedding.[50–56] We therefore consider transients between the desirable steady solution and the attractor, including the *descending* trajectory, which is slowly driven from the attractor to the steady solution, and the *ascending* trajectory, which is allowed to gradually return to the attractor. In both parts, the TKE changes at a slower rate than the natural, uncontrolled transient.

Details on the control used are deferred to the Appendix. The role of mean field models in flow control deserves and received dedicated investigations; examples include systems actuated by a volume force,[29,34] vertical oscillations,[32,33,35] and a synthetic jet.[36] Studies of the harmonically rotated cylinder, by Wesfreid, Protas, and collaborators,[38–40,57] also stress the dynamic role of mean field corrections. The present selection of the volume force aims to simplify the analytic burden of what is a side issue in this study. This selection is nonetheless generic, in view of the fact that other forms of (boundary) actuation are commonly represented in low order Galerkin models by actuation modes that mimic volume forces,[36,55,58–62] as well as the fact that the main impact of moderate levels of actuation on the mean field, in such models, is indirectly, through the Reynolds stresses associated with changes in unsteadiness, in the flow. We also note that, while very aggressive actuation would typically require richer mode sets to approximate both fast fluctuations (e.g., by additional POD modes) and mean field variations (by additional shift modes), the conclusions and tools elaborated here are applicable in such cases as well.

### C. Empirical base flow and fluctuation trajectories

The Reynolds decomposition[63] partitions the flow field as a sum of a mean flow $\overline{\mathbf{u}}$ and an unsteady fluctuation $\mathbf{u}'$. Fluid dynamics studies and reduced order models of turbulent flows typically focus on an attractor's unsteadiness, en-

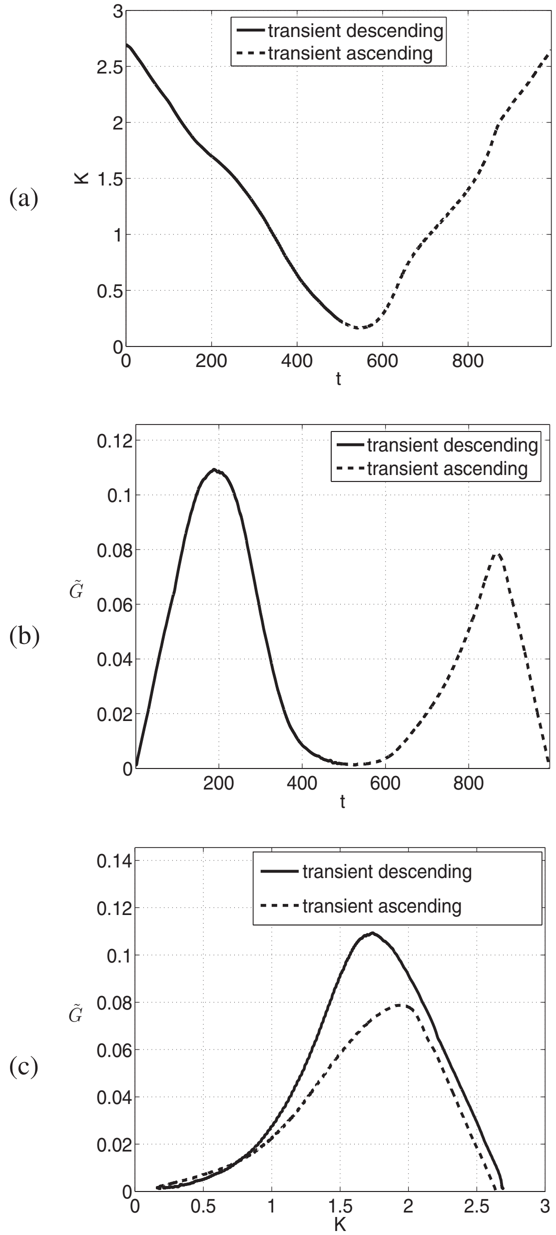


FIG. 3. (a) The time evolution of the fluctuation energy of the forced transient from the attractor toward the steady solution and back to the attractor. This transient is longer (and slower) than the natural transient. (b) The time evolution of the slowly varying amplitude $\tilde{G}$ of the oscillatory actuation $G=\tilde{G}\cos(\phi)$. A higher amplitude is needed to drive the descending trajectory toward the steady solution (—), than during the relaxation of the ascending second half (- -), as the flow gradually returns to the attractor. (c) To highlight that difference in the required actuation amplitude, $\tilde{G}$ is plotted as a function of the instantaneous fluctuation energy in the actuated descending trajectory (—) and the ascending trajectory (- -).

capsulated in $\mathbf{u}'$, whereby $\bar{\mathbf{u}}$ is typically fixed. Our focus on transient dynamics and on mean field variations motivates the substitution of the steady mean, $\bar{\mathbf{u}}$, by a slowly varying *base flow* $\mathbf{u}^B$. Thus

$$\mathbf{u} = \mathbf{u}^B + \mathbf{u}'. \tag{3}$$

This formalism agrees with the conventions of statistical fluid dynamics for statistically nonstationary processes.

Following Ref. 25, the assumed slow variation in the mean flow and of harmonically dominated fluctuations can be formalized by introducing a small parameter $1 \gg \epsilon > 0$ and slowly varying amplitude and frequency functions, $\mathbf{u}_0^B(\mathbf{x},\epsilon t)$, $\mathbf{u}_k^a(\mathbf{x},\epsilon t)$, $\mathbf{u}_k^b(\mathbf{x},\epsilon t)$, and $\omega(\epsilon t)$, such that

$$\mathbf{u}^B(\mathbf{x},t) = \mathbf{u}_0^B(\mathbf{x},\epsilon t), \tag{4a}$$

$$\mathbf{u}'(\mathbf{x},t) = \sum_{k=1}^{M} \{\mathbf{u}_k^a(\mathbf{x},\epsilon t)\cos[k\omega(\epsilon t)t] + \mathbf{u}_k^b(\mathbf{x},\epsilon t)\sin[k\omega(\epsilon t)t]\}, \tag{4b}$$

where $M$ is the number of significant temporal harmonics in the fluctuation. The reciprocal parameter $1/\epsilon$ is viewed as a time constant for variations that are slow, relative to the period $T:=2\pi/\omega$. Under the ansatz (4), we shall neglect time derivatives of order $O(\epsilon)$.

A preliminary processing need is to extract $\mathbf{u}^B$, $\mathbf{u}_k^a$, and $\mathbf{u}_k^b$ from empirical flow data, using the ansatz (4):

$$\mathbf{u}^B(\mathbf{x},t) = \frac{1}{T}\int_{t-(T/2)}^{t+(T/2)} d\tau\, \mathbf{u}(\mathbf{x},\tau), \tag{5a}$$

and

$$\mathbf{u}_k^a(\mathbf{x},\epsilon t) = \frac{2}{T}\int_{t-(T/2)}^{t+(T/2)} d\tau\, \mathbf{u}(\mathbf{x},\tau)\cos(k\omega\tau),$$
$$\mathbf{u}_k^b(\mathbf{x},\epsilon t) = \frac{2}{T}\int_{t-(T/2)}^{t+(T/2)} d\tau\, \mathbf{u}(\mathbf{x},\tau)\sin(k\omega\tau), \tag{5b}$$

yielding also a working definition of the TKE

$$\mathcal{K}(\epsilon t) = \tfrac{1}{2}\|\mathbf{u}'(\cdot,\epsilon t)\|_\Omega^2 = \tfrac{1}{2}\|\mathbf{u}(\cdot,\epsilon t) - \mathbf{u}^B(\cdot,\epsilon t)\|_\Omega^2. \tag{5c}$$

Here the norm $\|\ \|_\Omega$ corresponds to the inner product in the Hilbert space of square-integrable functions $\mathcal{L}_2(\Omega)$:

$$(\mathbf{u},\mathbf{v})_\Omega = \int_\Omega d\mathbf{x}\, \mathbf{u}\cdot\mathbf{v}. \tag{6}$$

Estimating the period $T$, which may vary slowly but substantially along transients, is an implicit challenge in Eq. (5). A simple heuristic is applicable to harmonically dominated flows, where the dominant POD mode pair represents the first temporal harmonic. Along the natural transient, the corresponding POD mode amplitudes evolve as $a_1 = r\cos(\phi)$ and $a_2 = r\sin(\phi)$, with slowly varying $r$ and $\omega = \dot{\phi}$. Moreover, away from the steady solution, $\mathbf{u}_s$, period averages $\bar{a}_i$ are negligible relative to $r$. Thus, one can estimate $\phi := \angle(a_1 + \imath a_2)$, extract $\omega(\epsilon t)$ as the slope of a straight line approximation of $\phi$ over a moving, fixed length time window $[t-(T_0/2), t+(T_0/2)]$ [with $T_0 > \max(T)$], and define the instantaneous period as $T(\epsilon t) := 2\pi/\omega(\epsilon t)$. Near the steady solution, denoted as $\mathbf{u}_s$, the period is known from linear stability analysis.

The spatial symmetry of the cylinder wake facilitates the computations of Eq. (5), in that configuration: define the *symmetric* and *antisymmetric* fields as

$$u^{\mathrm{sym}}(x,y):=\tfrac{1}{2}[u(x,y)+u(x,-y)],$$

$$v^{\mathrm{sym}}(x,y):=\tfrac{1}{2}[v(x,y)-v(x,-y)],$$

$$u^{\mathrm{asym}}(x,y):=\tfrac{1}{2}[u(x,y)-u(x,-y)],$$

$$v^{\mathrm{asym}}(x,y):=\tfrac{1}{2}[v(x,y)+v(x,-y)].$$

In these terms, POD modes representing odd harmonics of the flow contribute only to $\mathbf{u}^{\mathrm{asym}}$, and those representing even harmonics and the mean field only to $\mathbf{u}^{\mathrm{sym}}$. Residual errors in Eq. (5) are therefore reduced when $\mathbf{u}$ is substituted accordingly by either $\mathbf{u}^{\mathrm{sym}}$ or $\mathbf{u}^{\mathrm{asym}}$. Likewise, the overwhelming dominance of $\mathbf{u}'$ by the first harmonic allows us to approximate $\mathbf{u}'=\mathbf{u}^{\mathrm{asym}}$ in Eq. (5c).

## III. MEAN FIELD THEORY

This section presents a first principles perspective on the need to include mean field dynamics in low order Galerkin models and on the form of such models. The analytic arguments are reviewed in Sec. III B. A novel modal transient modal energy flow analysis in Sec. III C demonstrates that the contribution of mean field variations to the dynamic forces in the NSE is indeed essential. That analysis also shows that the kinematic shift mode from Ref. 17 (see also GKSM 1, below), arguably the crudest mean field model, provides a good approximation of the dynamic effects of the DNS-based mean flow. This observation suggests a dynamic equivalence between the empirical-kinematic and analytic-dynamic shift mode definitions, and justifies the use of the former, which is much easier to compute. The discussion begins in Sec. III A with an examination of a simple, motivating example. It is used to establish ties with our earlier work,[17] where the shift mode and the kinematic approach to Galerkin mean field models were first introduced, and with prevalent model reduction methods for fluid flow systems.

### A. A simple motivating example

We consider a minimal Galerkin model that approximates oscillatory instabilities arising from supercritical (soft) bifurcations[17]

$$\frac{d}{dt}\begin{bmatrix} a_1 \\ a_2 \\ a_3 \end{bmatrix} = \begin{bmatrix} \sigma-\beta a_3 & -\omega-\gamma a_3 & 0 \\ \omega+\gamma a_3 & \sigma-\beta a_3 & 0 \\ \alpha a_1 & \alpha a_2 & -\sigma_\Delta \end{bmatrix}\begin{bmatrix} a_1 \\ a_2 \\ a_3 \end{bmatrix} + \begin{bmatrix} 1 \\ 0 \\ 0 \end{bmatrix} b, \qquad (7)$$

$$s=a_1.$$

Here $\mathbf{a}=[a_1,a_2,a_3]^T$ is the state, $b$ is a control command, and $s$ is an output (e.g., a sensor signal). $\sigma$, $\sigma_\Delta$, and $\omega$ represent parameters characterizing the linear instability, while $\alpha$, $\beta$, and $\gamma$ parameterize the nonlinearity.

The following are straightforward observations:

- $\mathbf{a}_s=0$ is an unstable fixed point when $b=0$.
- Unactuated transients converge to a limit cycle

$$a_1^{\bigcirc}(t)=\sqrt{\sigma\sigma_\Delta/\alpha\beta}\cos(\omega^{\bigcirc}t),$$

$$a_2^{\bigcirc}(t)=\sqrt{\sigma\sigma_\Delta/\alpha\beta}\sin(\omega^{\bigcirc}t), \qquad (8)$$

$$a_3^{\bigcirc}(t)=\sigma/\beta,$$

  where $\omega^{\bigcirc}=\omega+\gamma\sigma/\beta$ is the post-transient frequency.
- Natural transients are characterized by growing oscillations in $a_1$ and $a_2$, and a slow, nonoscillatory transient in $a_3$, tracking $2\alpha\mathcal{K}/\sigma_\Delta$. Here $\mathcal{K}:=1/2(a_1^2+a_2^2)$ is the oscillation energy.
- The nonlinear coupling between the oscillatory and nonoscillatory states is dynamically essential to represent both the instability of the origin, the varying growth rates and the convergence to an attractor.

As shown in Refs. 17 and 29, the state-space dynamics and the input-output (I/O) behavior described by Eq. (7) are essentially equivalent to those of a least-order Galerkin representation of the postbifurcation cylinder wake benchmark, as described in Sec. II. Here, $b$ takes the role of the (scaled) volume-force modulation amplitude $G$ in Eq. (1), and $s$ is a high-pass filtered version of a velocity sensor signal. Similar models represent other flow configurations, including wake flows and separated flows over airfoils at high angles of attack,[36,64,65] as well as combustion instabilities.[66,67]

We shall now examine three approaches that are commonly employed to derive reduced order Galerkin models for fluid flow systems, and use this examination to demonstrate the possible shortcomings of models that do not include base flow dynamics: models based on linear stability eigenmodes of the linearized system at the steady solution (i.e., the origin), POD approximation of the attractor, and balanced POD, based on either of these operating points.

We start with approximations based on linearizations around the fixed point at the origin. There is no trace of the quadratic term of Eq. (7) in the linearized system

$$\frac{d}{dt}\begin{bmatrix} a_1' \\ a_2' \\ a_3' \end{bmatrix} = \begin{bmatrix} \sigma & -\omega & 0 \\ \omega & \sigma & 0 \\ 0 & 0 & -\sigma_\Delta \end{bmatrix}\begin{bmatrix} a_1' \\ a_2' \\ a_3' \end{bmatrix} + \begin{bmatrix} 1 \\ 0 \\ 0 \end{bmatrix} b, \qquad (9)$$

$$s'=a_1'.$$

where we use a prime to represent the modeled (small) state perturbations from the nominal operating point or orbit. The number of parameters drop from six to three, indicating a loss of information. Furthermore, the dynamics of Eq. (9) is decomposed into two, uncoupled invariant subspaces. The first is span$\{\mathbf{e}_1,\mathbf{e}_2\}$. (Here we use the standard notation of the natural basis, where $\mathbf{e}_i\in\Re^n$ is defined by $\mathbf{e}_i=[0,\dots,0,1,0,\dots,0]^T$, with the entry 1 in the $i$th place.) The dynamics of $a_1'$ and $a_2'$ are captured by the compression to the invariant subspace span$\{\mathbf{e}_1,\mathbf{e}_2\}$. This subspace is controllable, observable, and open-loop antistable with an exponential growth rate of $\sigma$. The second invariant subspace is span$\{\mathbf{e}_3\}$. It represents the exponentially stable dynamics of

$a_3'$ which is neither controlled, nor sensed in the linearized model.

The span of the unstable eigenmodes is therefore span$\{\mathbf{e}_1, \mathbf{e}_2\}$. A model based on the Galerkin projection of Eq. (7) on this subspace, using the origin as a base flow, postulates an approximation of the form

$$\mathbf{a}(t) = a_1(t)\mathbf{e}_1 + a_2(t)\mathbf{e}_2. \tag{10}$$

It leads to the reduced order model

$$\frac{d}{dt}\begin{bmatrix} a_1' \\ a_2' \end{bmatrix} = \begin{bmatrix} \sigma & -\omega \\ \omega & \sigma \end{bmatrix}\begin{bmatrix} a_1' \\ a_2' \end{bmatrix} + \begin{bmatrix} 1 \\ 0 \end{bmatrix} b, \qquad s' = a_1'. \tag{11}$$

This model provides a good initial approximation of transients, near the origin, but wrongly predicts an unlimited exponential growth, rather than the actual settling on the attractor.

Next, we consider balanced truncation model reduction. In its original form, this method is applicable to stable linear systems. A common way to apply it to unstable systems is to partition the state space into the invariant exponentially stable and the unstable subspaces, including so-called marginally stable modes associated with pure oscillations. Model reduction is then applied only to the stable component of the system. Here, the stable subspace in Eq. (9) is neither controllable nor observable, and is invariant under both the linearized system and its adjoint. Model reduction, based on an I/O perspective, is therefore bound to ignore the stable subspace span$\{\mathbf{e}_3\}$ and lead once again to the reduced order system (11), with the shortcomings noted above.

A standard POD analysis and POD model will focus on the hyperplane spanned by the attractor. Here the attractor mean, $\overline{\mathbf{a}} = (\sigma/\beta)\mathbf{e}_3$, serves as an origin. As is easy to see, the dominant POD modes are, again, $\mathbf{e}_1$ and $\mathbf{e}_2$. The POD approximation is therefore of the form

$$\mathbf{a}(t) = \bar{a}_3\mathbf{e}_3 + a_1(t)\mathbf{e}_1 + a_2(t)\mathbf{e}_2, \tag{12}$$

where $\bar{a}_3 = \sigma/\beta$. The projection of the original system (7) on the hyperplane formed by such approximations leads to the following Galerkin system

$$\frac{d}{dt}\begin{bmatrix} a_1 \\ a_2 \end{bmatrix} = \begin{bmatrix} 0 & -\omega^{\circ} \\ \omega^{\circ} & 0 \end{bmatrix}\begin{bmatrix} a_1 \\ a_2 \end{bmatrix} + \begin{bmatrix} 1 \\ 0 \end{bmatrix} b, \qquad s = a_1. \tag{13}$$

This ideal oscillator model fails on several accounts. First, it identifies the unactuated steady solution with the attractor's mean, which is not a fixed point of the original flow. Second, it does not predict the instability of the steady solution. Third, it does not determine the convergence to a single attractor, characterized by one specific oscillations amplitude, namely, $\sqrt{\sigma\sigma_\Delta/\alpha\beta}$. Finally, the system (13) is structurally unstable and arbitrarily small numerical perturbations of its coefficients can render it either exponentially stable or antistable.

Summarizing our observations to this point, each of the three Galerkin approximation approaches considered above failed because it leads to a reduced order model in a hyperplane spanned by $\mathbf{e}_1$ and $\mathbf{e}_2$ alone, ignoring the orientation $\mathbf{e}_3$ of slow changes in the mean field. Indeed, in both the first two approaches, this shortfall is an intrinsic property of the method. The only remedy to this shortcoming is the reinclusion of the orientation of the mean field correction $\mathbf{e}_3 \propto \overline{\mathbf{a}} - \mathbf{a}_s$. In a nutshell, that is the message of Ref. 17.

Indeed, the counterpart observation in the context of the wake flow benchmark would be the inclusion in the expansion set of a shift mode representing the global mean field correction

$$\mathbf{u}_\Delta \propto \mathbf{u}_0 - \mathbf{u}_s, \tag{14}$$

where $\mathbf{u}_s$ is the steady solution and $\mathbf{u}_0$ is the attractor's mean flow. This geometrical approach, repeated for completeness in GKSM 1, below, was proposed in Ref. 17 and used in a succession of flow control studies, cited in Sec. I. While the considerations leading to the introduction of the shift mode were clearly rooted in issues of dynamic representation, we nonetheless term the specific definition (14) a *kinematic* shift mode. We do so to contrast this derivation from kinematic data, with methods based on a direct utilization of the governing NSE, as discussed in Sec. III B below.

Following Ref. 15, the last approximation we consider here is the balanced POD approximation, based on the attractor $\mathbf{a}^{\circ}(t)$ as a periodic linearization reference. Using the notations of Eq. (8) for the attractor trajectory, the perturbed state is defined as $\mathbf{a}'(t) := \mathbf{a}(t) - \mathbf{a}^{\circ}(t)$. In these terms, the periodically time varying linearization is

$$\frac{d}{dt}\begin{bmatrix} a_1' \\ a_2' \\ a_3' \end{bmatrix} = \begin{bmatrix} 0 & -\omega^{\circ} & -(\beta a_1^{\circ} + \gamma a_2^{\circ}) \\ \omega^{\circ} & 0 & -(\beta a_2^{\circ} - \gamma a_1^{\circ}) \\ 2\alpha a_1^{\circ} & 2\alpha a_2^{\circ} & -\sigma_\Delta \end{bmatrix}\begin{bmatrix} a_1' \\ a_2' \\ a_3' \end{bmatrix} + \begin{bmatrix} 1 \\ 0 \\ 0 \end{bmatrix} b, \qquad s' = a_1'. \tag{15}$$

As outlined in Ref. 15 (see also Ref. 68), the analysis of this periodic system can be carried, equivalently, in the context of the *lifted* system. The lifting technique traces back to work on periodic and delay systems.[69] It attained its current title in the context of studies of robust control of sample data systems.[70,71] The idea is to substitute the periodic, continuous time system with a time invariant discrete time system with distributed inputs and outputs based on periodic state sampling. Leaving out technical details, the fact that the dynamics over the subspace spanned by $\mathbf{e}_3$ is coupled with that of the other two state components means that this method does not lead to neglecting span$\{\mathbf{e}_3\}$ as an intrinsic property. The same holds for balancing the linearization about attenuated controlled attractors, e.g., using the counterpart of the dissipative control described in the Appendix. The failure of the balanced truncation based on the linearization about the origin is, in this sense, a singular, nongeneric deviation. Nonetheless, we note that balanced POD model reduction does not guarantee the inclusion of the essential mean field correction in the expansion set. Various possible remedies include the use of local reductions and parameterized families of local mode sets, as in Refs. 34 and 49, or the inclusion of the shift mode coefficient in the output equation for the purpose of balancing. In particular, an *a priori* awareness and computation of the shift mode are essential.

### B. The NSE perspective

In this section, we explore the need for a Galerkin mean field model and derive its form. When compared with the original presentation, in Ref. 17, the contribution, both here and in Sec. III C, is in the direct appeal to the NSE (2), which encapsulates the dynamics' first principles. A simplifying axiomatic framework, distilled from properties of the cylinder wake flow and aimed to facilitate the analysis, is delineated in Sec. III B 1. It is used in Sec. III B 2 to establish the need to account for mean field variations, and in Sec. III B 3, to derive an NSE-based definition of a local shift mode. Closing the discussion in Sec. III B 4, we comment on the generality of the observations in Secs. III B 2 and III B 3. A modal energy flow analysis of transient dynamics will be introduced in Sec. III C and will provide a detailed quantitative demonstration of the arguments made here.

#### *1. An axiomatic framework and filtered partition of the NSE*

We analyze the system under three hypotheses that reflect a focus on a distinct temporal frequency in the flow. All three hypotheses provide a good approximation of the observed phase-averaged behavior of the natural and actuated cylinder wake flow benchmark, as described in Sec. II and elaborated in detail in Ref. 17.

*a. Assumption NSE 1.* The flow is dominated by a slowly varying base flow $\mathbf{u}^B$, and a periodic, zero mean fluctuation $\mathbf{u}'$, with a slowly varying periodic characteristics, as in Eqs. (3) and (4) with $M=1$.

*b. Assumption NSE 2.* The force field $\mathbf{f}$ is of the form (4b), with $M=1$ and the same frequency as $\mathbf{u}'$.

*c. Assumption NSE 3. A Krylov–Bogoliubov phase invariance hypothesis.* The TKE of both the natural and the actuated flow is slowly varying. In particular, the second temporal harmonic of $\mathcal{K}(t)$ is negligible.

The focus on a single dominant harmonic is done for simplicity, and we shall comment briefly on the effects of multiple harmonics along the presentation and summarized in Sec. III B 4. A discussion of the mean field model for a system under (boundary) actuation at another, possibly unrelated frequency, can be found in Ref. 36.

We shall now consider the temporal partition of the NSE (2b), as an interaction of a base flow equation and a dominant harmonic equation.

*d. The base flow equation.* This is the familiar RANSE. It describes the dependence of the mean field $\mathbf{u}^B$ on the fluctuation $\mathbf{u}'$. A computational approximation, valid under NSE 1, NSE 2, and NSE 3, is the average over a single period, moving time window (5a), denoted by an overline

$$\nabla \cdot (\mathbf{u}^B \otimes \mathbf{u}^B) + \nabla \cdot \overline{(\mathbf{u}' \otimes \mathbf{u}')} + \nabla \bar{p} - \frac{1}{\mathrm{Re}} \Delta \mathbf{u}^B = 0. \tag{16a}$$

The suppression of terms neglected in Eq. (16a) is justified by the axioms NSE 1, NSE 2, and NSE 3: the sinusoidal behavior of both $\mathbf{u}'$ and $\mathbf{f}$ means that the terms $\nabla \cdot (\mathbf{u}^B \otimes \mathbf{u}')$, $\nabla \cdot (\mathbf{u}' \otimes \mathbf{u}^B)$, and $\mathbf{f}$ in Eq. (2b) average to zero over each shedding period. The stipulation (4a) means that the time derivative, $\partial_t \mathbf{u}^B$, is of order $O(\epsilon)$ and can be neglected in Eq. (16a).

We pay special attention to the Reynolds stress:

$$\begin{aligned}\nabla \cdot \overline{(\mathbf{u}' \otimes \mathbf{u}')} &= \frac{1}{T} \nabla \cdot \int_{t-(T/2)}^{t+(T/2)} d\tau\, \mathbf{u}'(\mathbf{x},\tau) \otimes \mathbf{u}'(\mathbf{x},\tau) \\ &= \frac{1}{2} \nabla \cdot (\mathbf{u}_1^a \otimes \mathbf{u}_1^a + \mathbf{u}_1^b \otimes \mathbf{u}_1^b).\end{aligned} \tag{16b}$$

The second equality in Eq. (16b) is the result of eliminating by window averaging the product of temporally orthogonal trigonometric functions in Eq. (4b).

*e. The fluctuation equation.* Window averaging is substituted here by Eq. (5b) with $k=1$, i.e., the projection on the first temporal harmonic

$$\partial_t \mathbf{u}' + \nabla \cdot (\mathbf{u}' \otimes \mathbf{u}^B + \mathbf{u}^B \otimes \mathbf{u}') + \nabla p' - \frac{1}{\mathrm{Re}} \Delta \mathbf{u}' - \mathbf{f} = 0. \tag{16c}$$

The terms $\nabla \cdot (\mathbf{u}^B \otimes \mathbf{u}^B)$ and $\nabla \cdot (\mathbf{u}' \otimes \mathbf{u}')$ comprise of a slowly varying and a second harmonic components, and are eliminated by the projection (5b). Equation (16c) is a variant Reynolds equation, where a constant weight is substituted by a sinusoidal weight in the averaging over a moving time window.

*f. TKE evolution.* The time evolution of the TKE, $\mathcal{K}(t)$, is key to understanding the dynamics of the system. The general dynamic law, governing $\mathcal{K}$, is of the form:[72,73]

$$\frac{d}{dt}\mathcal{K} = \mathcal{P} = \mathcal{P}_p + \mathcal{P}_d + \mathcal{P}_c + \mathcal{P}_t + \mathcal{P}_{\mathrm{pr}} + \mathcal{P}_a, \tag{17}$$

where $\mathcal{P}_p$, $\mathcal{P}_d$, $\mathcal{P}_c$, $\mathcal{P}_t$, $\mathcal{P}_{\mathrm{pr}}$, and $\mathcal{P}_a$ are the respective production, dissipation, convection, transfer, pressure and actuation components of the supplied power $\mathcal{P}$:

$$\mathcal{P}_p = -\overline{[\mathbf{u}', \nabla \cdot (\mathbf{u}' \otimes \mathbf{u}^B)]_\Omega}, \tag{18a}$$

$$\mathcal{P}_c = -\overline{[\mathbf{u}', \nabla \cdot (\mathbf{u}^B \otimes \mathbf{u}')]_\Omega}, \tag{18b}$$

$$\mathcal{P}_t = -\overline{[\mathbf{u}', \nabla \cdot (\mathbf{u}' \otimes \mathbf{u}')]_\Omega}, \tag{18c}$$

$$\mathcal{P}_d = \frac{1}{\mathrm{Re}} \overline{(\mathbf{u}', \Delta \mathbf{u}')_\Omega}, \tag{18d}$$

$$\mathcal{P}_{\mathrm{pr}} = -\overline{(\mathbf{u}', \nabla p')_\Omega}, \tag{18e}$$

$$\mathcal{P}_a = \overline{(\mathbf{u}', \mathbf{f})_\Omega}. \tag{18f}$$

This section closes with implications of the axiomatic framework on the various terms of Eq. (18).

To begin with, note that $\mathcal{P}_t \approx 0$ neglecting first and higher harmonics in Eq. (18c). It is also well established (see, e.g., Refs. 16 and 74) that $\mathcal{P}_{\text{pr}} \approx 0$ in the cylinder wake flow. (Section III B 4 comments on the cases where $\mathcal{P}_{\text{pr}} \not\approx 0$.) Phase averaging is the key to simplifying the remaining terms. In relation to actuation, NSE 2 means that the volume-force amplitude can be written as

$$G(t) = \tilde{G}(\epsilon t)\cos[\omega(\epsilon t)t + \theta(\epsilon t)], \quad \tilde{G} \geq 0. \tag{19}$$

Invoking NSE 1 for the velocity field, the TKE becomes

$$\begin{aligned}\mathcal{K}(t) &= \tfrac{1}{2}\|\mathbf{u}'(\cdot,\epsilon t)\|_\Omega^2 \\ &= \tfrac{1}{2}\|\mathbf{u}_1^a(\cdot,\epsilon t)\cos(\omega t) + \mathbf{u}_1^b(\cdot,\epsilon t)\sin(\omega t)\|_\Omega^2,\end{aligned} \tag{20}$$

where we use the $\mathcal{L}_2(\Omega)$ norm. The phase invariance assumption, NSE 3, means that $\mathcal{K}(t)$ is unaffected by phase shifts, $\omega t \mapsto \omega t + \theta$, in Eq. (20). Consequently,

$$\mathcal{K} = \tfrac{1}{2}\|\mathbf{u}_1^a\|_\Omega^2 = \tfrac{1}{2}\|\mathbf{u}_1^b\|_\Omega^2 \quad \text{and} \quad (\mathbf{u}_1^a, \mathbf{u}_1^b)_\Omega = 0. \tag{21}$$

It will be convenient to normalize $\mathbf{u}_1^a$ and $\mathbf{u}_1^b$, as

$$\begin{gathered}\mathbf{u}^a := \frac{1}{\sqrt{2\mathcal{K}}}\mathbf{u}_1^a \quad \text{and} \quad \mathbf{u}^b := \frac{1}{\sqrt{2\mathcal{K}}}\mathbf{u}_1^b, \\ \Updownarrow \\ \mathbf{u}_1^a = \sqrt{2\mathcal{K}}\mathbf{u}^a \quad \text{and} \quad \mathbf{u}_1^b = \sqrt{2\mathcal{K}}\mathbf{u}^b.\end{gathered} \tag{22}$$

In particular, up to state-space rotation, $\mathbf{u}^a$ and $\mathbf{u}^b$ are the POD modes of the period $[t-(T/2), t+(T/2)]$, making Eq. (4) equivalent to a temporally local POD approximation.

Using Eqs. (1), (19), and (22), the phase-averaged equation (18) becomes

$$\begin{aligned}\mathcal{P}_p &= \kappa_p(\mathbf{u}^a,\mathbf{u}^b,\mathbf{u}^B)\cdot\mathcal{K}, \\ \mathcal{P}_c &= \kappa_c(\mathbf{u}^a,\mathbf{u}^b,\mathbf{u}^B)\cdot\mathcal{K}, \\ \mathcal{P}_t &= 0, \\ \mathcal{P}_d &= \kappa_d(\mathbf{u}^a,\mathbf{u}^b)\cdot\mathcal{K}, \\ \mathcal{P}_{\text{pr}} &= 0, \\ \mathcal{P}_a &= \kappa_a(\mathbf{u}^a,\mathbf{u}^b,\mathbf{g})\cdot\tilde{G}\cdot\sqrt{\mathcal{K}},\end{aligned} \tag{23}$$

where $\kappa_p$, $\kappa_c$, $\kappa_d$, and $\kappa_a$ are functions of the modes in the argument list. With constant POD modes, temporal dependence enters due to the evolution of the base flow $\mathbf{u}^B$ and of the TKE $\mathcal{K}$.

In summary, the axiomatic framework shapes Eq. (17) as

$$\frac{d}{dt}\mathcal{K} = \kappa_n(\mathbf{u}^a,\mathbf{u}^b,\mathbf{u}^B)\cdot\mathcal{K} + \kappa_a(\mathbf{u}^a,\mathbf{u}^b,\mathbf{g})\cdot\tilde{G}\cdot\sqrt{\mathcal{K}}, \tag{24}$$

where the subscripts "$n$" and "$a$" indicate the natural (i.e., unactuated) and the actuated components.

#### 2. The need for a mean field representation

Consider the natural transient, where Eq. (24) becomes

$$\frac{d}{dt}\mathcal{K} = \kappa_n(\mathbf{u}^a,\mathbf{u}^b,\mathbf{u}^B)\cdot\mathcal{K}. \tag{25}$$

Equation (25) needs to accommodate the following properties:

- A linearly unstable fixed point at $\mathbf{u}_s$, where $\mathcal{K}=0$.
- Growth of $\mathcal{K}$ along the natural transient.
- A fixed point with $\mathcal{K}_* > 0$, on the attractor.
- Decay of perturbations from the attractor.

These requirements are abbreviated as

$$\mathcal{P} = \kappa_n\mathcal{K}\begin{cases} =0, & \mathcal{K}=0, \\ >0, & \mathcal{K}\in(0,\mathcal{K}_*), \\ =0, & \mathcal{K}=\mathcal{K}_*, \\ <0, & \mathcal{K}>\mathcal{K}_*. \end{cases} \tag{26}$$

An implicit restriction is on the states along the natural transient/attractor and on the small perturbations thereof, where our framework is valid. By Eq. (26), $\kappa_n$ must vary with the operating condition. Specifically,

$$\kappa_n(\mathbf{u}^a,\mathbf{u}^b,\mathbf{u}^B)\begin{cases} >0, & \mathcal{K}\in[0,\mathcal{K}_*), \\ =0, & \mathcal{K}=\mathcal{K}_*>0, \\ <0, & \mathcal{K}>\mathcal{K}_*. \end{cases} \tag{27}$$

In a standard POD Galerkin approximation, however, the operating-point dependent modes $\mathbf{u}^a$ and $\mathbf{u}^b$ are substituted by the fixed POD modes. Should variations in the base flow $\mathbf{u}^B$ be ignored as well, the coefficient $\kappa_n$ will become constant and the three conditions in Eq. (27) be mutually exclusive! That is, the suppression of the dependence of $\kappa_n$ on the base flow then leads to precisely the same pitfalls observed in the analysis of the minimal Galerkin system, in Sec. III A: the inability to adjust the growth rate $\kappa_n$ along a transient plays the same role as the inability to adjust the growth rate $\sigma-\beta a_3$ in Eq. (7).

Let us recap: the flow is governed by a bilateral coupling of the Reynolds and fluctuation equations (16a) and (16c). Variations in $\mathbf{u}'$, hence in the Reynolds stress (16b), modify $\mathbf{u}^B$ in Eq. (16a). In turn, adjustments of $\mathbf{u}^B$ are encoded by the quadratic term $\nabla\cdot(\mathbf{u}'\otimes\mathbf{u}^B+\mathbf{u}^B\otimes\mathbf{u}')$, in Eq. (16c), as modifications of the linear growth rate and oscillation frequency in $\mathbf{u}'$. A formal analysis of the energy flow equation demonstrated that a representation of both components of these bilateral interactions is essential. In contrast, the traditional approach to POD modeling is focused solely on a reduced order representation of Eq. (16c) and uses a fixed base flow. This implies that the traditional POD model is inherently incapable to adequately represent the flow's dynamics. This conclusion explains pervasive difficulties with POD models and will be demonstrated quantitatively in Sec. III C. In Sec. III B 4, we will comment on the reconciliation of this observation with the apparent existence of many POD success stories.

The analysis also highlights the need to account for the transient deformation of the dominant fluctuation modes, $\mathbf{u}^a$ and $\mathbf{u}^b$, which is ignored in standard POD models, but is reflected in changes in the growth rates $\kappa_n$ and elsewhere. While not central in this article, this issue will come to light and its significance be quantified in the modal energy flow analysis in Sec. III C. The authors elaborated on the role of mode deformations in Refs. 34, 49, and 75. Related observations were made by a number of other authors, e.g., Refs. 35 and 76–78.

#### *3. An NSE-based shift mode definition*

Consider a small perturbation $\delta\mathbf{u}_1^a(\mathbf{x},\epsilon t)$ and $\delta\mathbf{u}_1^b(\mathbf{x},\epsilon t)$ in the dominant oscillatory modes:

$$\delta\mathbf{u}'(\mathbf{x},t) = \delta\mathbf{u}_1^a(\mathbf{x},\epsilon t)\cos(\omega t) + \delta\mathbf{u}_1^b(\mathbf{x},\epsilon t)\sin(\omega t).$$

Neglecting terms that are quadratic in perturbations, the approximate contribution to the Reynolds stress is then

$$\begin{aligned}\nabla\cdot\overline{(\delta\mathbf{u}'\otimes\mathbf{u}'+\mathbf{u}'\otimes\delta\mathbf{u}')}&=\nabla\cdot\frac{1}{T}\int_{t-(T/2)}^{t+(T/2)}[d\tau\delta\mathbf{u}'(\mathbf{x},\tau)\otimes\mathbf{u}'(\mathbf{x},\tau)\\&\quad+\mathbf{u}'(\mathbf{x},\tau)\otimes\delta\mathbf{u}'(\mathbf{x},\tau)]\\&=\frac{1}{2}\nabla\cdot[\delta\mathbf{u}_1^{a\prime}\otimes\mathbf{u}_1^{a\prime}+\mathbf{u}_1^{a\prime}\otimes\delta\mathbf{u}_1^{a\prime}\\&\quad+\delta\mathbf{u}_1^{b\prime}\otimes\mathbf{u}_1^{b\prime}+\mathbf{u}_1^{b\prime}\otimes\delta\mathbf{u}_1^{b\prime}].\end{aligned}\tag{28}$$

The perturbation of the Reynolds stress is associated with a perturbation $\delta\mathbf{u}^B$ of the base flow, which satisfies the linearized Reynolds equation:

$$\begin{aligned}&\nabla\cdot(\delta\mathbf{u}^B\otimes\mathbf{u}^B+\mathbf{u}^B\otimes\delta\mathbf{u}^B)+\nabla\cdot\overline{(\delta\mathbf{u}'\otimes\mathbf{u}'+\mathbf{u}'\otimes\delta\mathbf{u}')}\\&\quad+\nabla\overline{\delta p}-\frac{1}{\mathrm{Re}}\Delta\delta\mathbf{u}^B=0.\end{aligned}\tag{29}$$

This equation is a first principles definition of a local mean field correction; i.e., a local shift mode

$$\mathbf{u}_\Delta \propto \delta\mathbf{u}^B.$$

We shall revisit this and related definitions, in Sec. IV.

#### *4. The generality of our conclusions*

In closing, we examine the generality of the arguments and conclusions above when the axiomatic restrictions to a single dominant frequency is dropped. This is obviously called for, given the ubiquity of flows displaying far more complex behavior and, indeed, of successful POD models that do not explicitly include shift modes.

A generic property of low order Galerkin models is the restriction to a limited range of length scales and a temporal bandwidth. Thus, for sufficiently large $M$ and $T$, the Galerkin expansion is (approximately) invariant under the truncated windowed Fourier transform (4). (The caveat is that longer time windows, necessary to justify the "slow time variations" assumption, will filter out short-lived irregular phenomena, restricting the time-scale over which transients can be resolved by a point-wise approximation.) The assumption that a low order Galerkin model provides a viable dynamic representation therefore justifies the partition of the NSE as the coupled interaction of a low-pass filtered equation (i.e., the RANSE), and a multiharmonic, band-pass-filtered fluctuation equation, generalizing the partition (16).

A point of departure from the simplicity of the arguments in Sec. III B 2 is the generic presence of multiple harmonics (i.e., $M>1$) in Eq. (4b). Then, the mere structure of the NSE transfer term $\nabla\cdot(\mathbf{u}'\otimes\mathbf{u}')$ in the generalized equation (16c) does not necessitate a zero contribution of the transfer power $\mathcal{P}_t$ in Eq. (17). It is a standard observation, however, that even when the transfer term does not vanish, it is generically too small, and insufficient to explain the transition from positive linear growth, at $\mathbf{u}_s$, to a marginally stable attractor's energetic level.[79]

Concerning the argument that the linear growth rate needs to change, we appeal to the conceptual framework of finite-time thermodynamics in Galerkin flow models.[80,81] Here, one notes the complementary roles of the linear and the quadratic Galerkin terms in the flow's energy economy: TKE production and dissipation are the domain of the linear term. The quadratic Galerkin terms provide the mechanism for triadic loss-less modal energy exchanges. Nonequilibrium modal energy levels are determined as a balance of net modal production and dissipation rates and triadic redistribution rates. The generic change in linear production and dissipation rates, between $\mathbf{u}_s$ and the attractor, therefore, leads to a change in balanced modal energy levels, precluding a fixed linear term from explaining both the early transient- and near-attractor dynamics.

Indeed, an examination of POD success stories reveals a pattern whereby the focus of the model quality evaluation is commonly on near-attractor dynamics, where linear growth rates are adjusted by *eddy viscosities*.[22,82–84] Alternatively, cubic terms are included[22,83] to account for changes in the mean field, albeit in a more complex form than was allowed by the use of a shift mode. As predicted by the arguments presented here, the standard affine+quadratic POD model often fails, or severely distorts dynamic predictions for larger perturbations. A pertinent example, illustrated in Fig. 4, is the aforementioned eight-state cylinder wake model, which grossly underpredicts the natural transient growth rate and overpredicts the transient duration.[16,17] Even to that extent, the success of the POD model in Ref. 16 may be partially attributed to the use of *extended* POD (Ref. 85) modes, extracted from transients approaching the attractor, and therefore including traces of mean field variations.

In contrast, the inclusion of a shift mode in a three-state model with only two attractor POD modes leads to a drastic improvement in the predicted convergence time. The three-state model is of the form (7), and the improvement is precisely the result of the ability to dynamically adjust the growth rate in the oscillatory states $a_{1,2}$, due to changes in the shift mode coefficient, $a_3$, along transients. The growth rate in this case is still underpredicted and the attractor is overpredicted in the exact Galerkin projection. As will be demonstrated by the detailed modal energy flow analysis in Sec. III C, the reasons are precisely those highlighted in Sec. III B 2: the truncation of the energy cascade and the dynamic

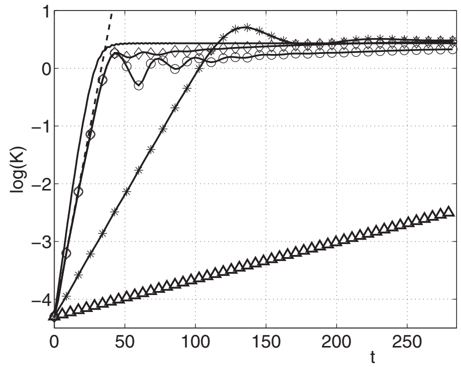


FIG. 4. Comparison of natural transient TKE predictions by a DNS simulation (—) and a number of low order POD models: an eight-mode traditional POD model (△), a least-order mean field model with the first attractor POD mode pair+1 shift mode (∗), a model including the two attractor POD modes, two linear stability modes, and a shift mode (○), and an 11-mode model, using eight POD modes, two stability modes, and one shift mode (◇). The dashed straight line indicates the linear stability growth rate at the steady solution.

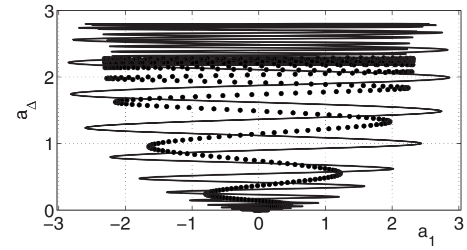


FIG. 5. Complementing Fig. 4, this figure compares transients of a DNS simulation (●) and of the three-state Galerkin model, based on the two attractor POD modes and the global kinematic shift mode (—). The phase portrait employs the amplitudes $a_1$ and $a_\Delta$ of the first POD and shift mode, respectively.

deformation of coherent structures. As seen in Fig. 4, including linear stability modes in the expansion, it is physically motivated which compensates for mode deformation, recovering the correct growth rate. This issue is discussed in more details in Refs. 34, 49, and 75. Figure 5 provides a clear view of the overprediction of the fluctuation level, relative to the approximate change in the mean field. Calibration of the three-state model can compensate for both dynamic effects at the Galerkin system level[32] but will not correct the reduced resolution effects of mode deformation.

In closing, we highlight two specific modifications of the simple framework discussed here, which may be necessary, in general. The first concerns the dimension of the mean field model. The shift mode is derived in Sec. III B 3 as a solution of the linearized Reynolds equation (29), and is determined by the perturbation of the Reynolds stress (16b), due to variations in $\mathbf{u}'$. When Eq. (4b) involves $M>1$ harmonics, each harmonic component contributes to a corresponding Reynolds stress term, $(1/2)\nabla\cdot(\mathbf{u}_i^a\otimes\mathbf{u}_i^a+\mathbf{u}_i^b\otimes\mathbf{u}_i^b)$. Unless it is justifiable to algebraically slave dynamics at higher harmonics to the dominant frequency, this allows up to $M$ degrees of freedom in the linearized Reynolds stress, leading up to $M$ independent shift modes.

Another point concerns flows where the pressure power is not negligible. The pressure force can be approximated by a linear[86] or a mixed linear-quadratic term in $\mathbf{u}'$ (Refs. 72 and 73; see also Ref. 87). This means that the period-averaged contribution of the pressure power will admit the same form as the production and convection terms, in 23, enabling the analysis to continue unaltered.

### C. Modal energy flow analysis

The net modal energy supply rates (i.e., modal power) determine the instantaneous growth rates of unsteadiness in each mode and in the flow. Energy flow rates also characterize the specific roles played by each mode in the mechanisms that govern flow dynamics, i.e., the extraction of energy from the mean flow, the dissipation and convection of TKE, the triadic intermodal energy transfer, and the effects of pressure work and of actuation on modal contributions to turbulent behavior. Concepts of energy flow rates are also at the foundation of a finite-time thermodynamic statistical closure theory, developed recently for Galerkin approximations.[80] Modal energy balance equations were derived and studied in Refs. 72 and 73 generalizing a framework established in Ref. 82.

The focus of modal energy flow analysis, to date, has mostly been on the attractor, where the compression of Eq. (17) to the Galerkin approximation becomes an algebraic, linear-quadratic equation. For example, time averaging the Galerkin-compressed equation (17), using empirical attractor data, yields a set of linear equations in the Galerkin system coefficients, which are useful to calibrate these coefficients.[36,73] In a departure from that past focus, we present here a first detailed energy flow analysis of the natural transient. This investigation will demonstrate the critical role of transient mean field variations, and will evaluate the quality of the approximation of the dynamic effect of mean field variations by a shift mode. It will also reveal the significance of other factors in the quality of Galerkin models, including dynamic mode deformation and the effects of truncation of low energy, high frequency modes.

Results are summarized in Figs. 6 and 7, presenting the predicted period-averaged power, $\mathcal{P}$, as a time evolution (top) and as a function of the TKE, $\mathcal{K}$ (bottom). The exact, DNS-based value of $\mathcal{P}$ is shown as a solid line in both figures. It is equivalently defined by Eq. (18), and by the numerical estimate, $\mathcal{P}:=(d/dt)\mathcal{K}$. The exact base flow, $\mathbf{u}^B$, and fluctuation field, $\mathbf{u}'$, are defined as in Eqs. (5a)–(5c).

Starting with Fig. 6, we compare the DNS-based value of $\mathcal{P}$ to values computed when $\mathbf{u}^B$ is substituted by the steady solution, $\mathbf{u}_s$ (dash-dotted curve), the attractor's mean, $\mathbf{u}_0$ (dashed curve), and by the dynamic estimate $\mathbf{u}_s+a_\Delta\mathbf{u}_\Delta$ (dotted curve), where $\mathbf{u}_\Delta$ is the shift mode from the normalized equation (14). In order to focus this figure solely on the dynamic effects of approximating or neglecting mean field variations, the value of $\mathcal{P}$ is computed in all cases with the exact fluctuation field.

Figure 6 brings the message of this section into sharp relief: ignoring mean field variations leads to drastic misrepresentation of the supplied power, hence the fluctuation growth rate. When $\mathbf{u}^B$ is substituted by the constant $\mathbf{u}_s$, the

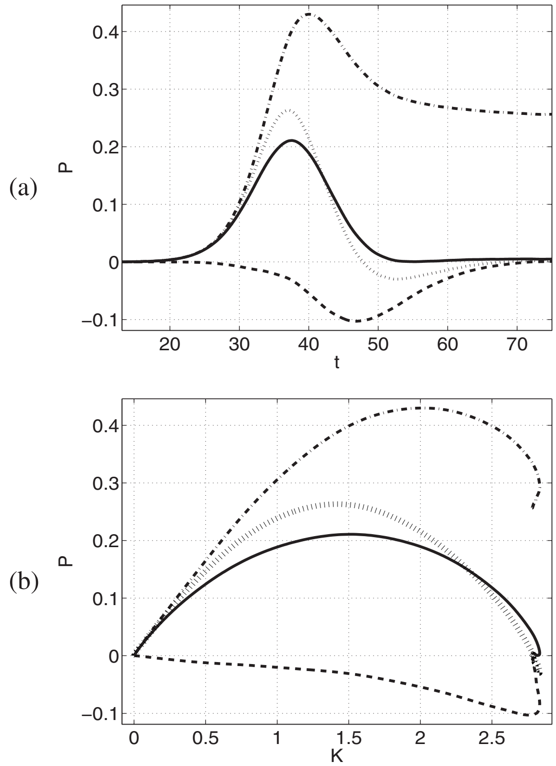


FIG. 6. First part of an energy flow analysis of the natural transient of the cylinder wake flow. (a) The total supplied power, $\mathcal{P}$, is plotted as a time evolution, (b) and as a function of the TKE level $\mathcal{K}$. The DNS value (solid curve) is compared with cases where the exact mean field $\mathbf{u}^B$ from Eq. (3) is substituted by the dynamic estimate $\mathbf{u}_s+a_\Delta\mathbf{u}_\Delta$ (dotted curve), where $\mathbf{u}_\Delta$ is the shift mode from the normalized equation (14), as well as by $\mathbf{u}_s$ (dash-dotted curve), and by $\mathbf{u}_0$ (dashed curve). In all cases $\mathcal{P}$ is computed with the same (exact) fluctuation field, $\mathbf{u}':=\mathbf{u}-\mathbf{u}^B$. Notice that the TKE overshoot in (b) corresponds to the overshoot in Fig. 2.

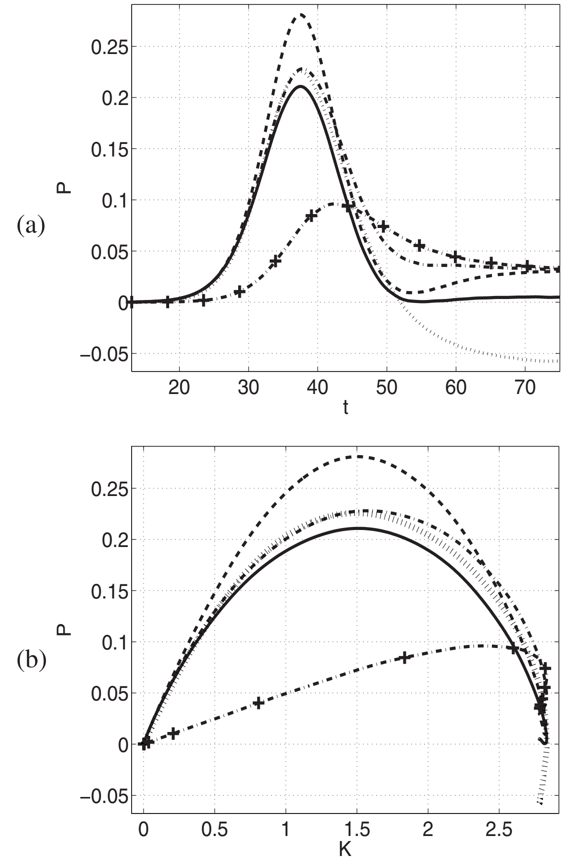


FIG. 7. Second part of an energy flow analysis of the natural transient of the cylinder wake flow, now comparing the exact value of $\mathcal{P}$ (solid curve) to estimates including Galerkin approximations of the fluctuation field $\mathbf{u}'$. Denoting by $\mathbf{u}^{a,b}$, $\mathbf{u}_s^{a,b}$, and $\mathbf{u}_0^{a,b}$ the respective pairs of local period POD modes, stability modes, and attractor POD modes, one estimate uses the exact (period-mean) base flow, $\mathbf{u}^B$, whereas $\mathbf{u}'$ is approximated by the projection on the local $\mathbf{u}^{a,b}$ (dashed curve). In the remaining three estimates, the base flow is substituted by $\mathbf{u}_s+a_\Delta\mathbf{u}_\Delta$ and the fluctuation field is approximated by its projections on $\mathbf{u}^{a,b}$ (dash-dotted curve), $\mathbf{u}_s^{a,b}$ (dotted curve), and $\mathbf{u}_0^{a,b}$ (dash-dot-plussed curve).

model more than doubles the predicted transient values of $\mathcal{P}$, and keeping $\mathcal{P}$ uniformly positive, precludes the existence of an attractor. Substituting $\mathbf{u}^B$ by $\mathbf{u}_0$ leads to the other extreme, where the Galerkin model predicts $\mathcal{P}<0$ over most of the true transient states, including the wrong prediction of a linear stability of $\mathbf{u}_s$. In contrast, a least-order estimate of mean field variations, employing a single shift mode, suffices to provide a decent approximation of $\mathcal{P}$ throughout the natural transient.

These results are complemented in Fig. 7, where the computation of $\mathcal{P}$ employs least-order Galerkin expansions of both $\mathbf{u}^B$ and $\mathbf{u}'$. The first estimate of $\mathcal{P}$ (dashed curve), is used to highlight the effect of truncating high harmonics in the least-order Galerkin approximation of $\mathbf{u}'$. This estimate therefore uses the exact value of $\mathbf{u}^B$ and an approximation of $\mathbf{u}'$ by the projection on the local, dominant POD mode pair of a single period, centered at the probed time instance. The use of local POD modes provides the best two-state approximation as it accounts for mode deformation along the transient. In the remaining three estimates, the base flow is substituted by the least-order Galerkin approximation $\mathbf{u}_s+a_\Delta\mathbf{u}_\Delta$, and the fluctuation field is approximated by its projections on the local POD modes (dash-dotted curve), the two stability modes (dotted curve), and the dominant POD mode pair of the attractor (dash-dot-crossed curve).

In examining Fig. 7, we first note that even the most accurate two-state Galerkin approximation of $\mathbf{u}'$ leads to an overprediction of $\mathcal{P}$, including $\mathcal{P}>0$ over the attractor. This validates the attribution of the overpredicted amplitude in Fig. 5 to the truncation of higher order modes (and harmonics) in the Galerkin model. As elaborated in Ref. 17, this overprediction is eliminated once higher order modes are included in the model. Notably, the substitution of $\mathbf{u}^B$ by $\mathbf{u}_s+a_\Delta\mathbf{u}_\Delta$, in both Figs. 6 and 7, has a smaller effect, whether the exact $\mathbf{u}'$ or its Galerkin approximation by the local POD modes, are used. The estimation error may increase when a fixed basis is used to approximate $\mathbf{u}'$, including the prediction of $\mathcal{P}<0$ near and over the attractor, when stability modes are used, and an underpredicted $\mathcal{P}$, throughout most of the transient, and $\mathcal{P}>0$ over the attractor, when attractor POD modes are used. These last distortions are attributed to mode deformation along transients[34,35,49,75,77] and are either partly offset or compounded with distortions due to the approximation of the base flow by $\mathbf{u}^B\approx\mathbf{u}_s+a_\Delta\mathbf{u}_\Delta$. Significantly, while accurate predictions require models to account for dynamic mode deformation, quantitative distortions due to

TABLE I. An overview of Sec. IV and the shift mode definitions described in Secs. IV A–IV D.

| | Kinematic | Dynamic |
|---|---|---|
| Principles | Data driven, using:<br>- POD approximate of base flow trajectory<br>- Global/local base flow increments | NSE driven, using:<br>- Increments in RANSE solutions<br>- Linearized NSE solutions |
| Global | Sec. IV A<br>**GKSM 1:** global increment of the base flow<br>**GKSM 2:** the dominant POD mode of the entire base flow transient | Sec. IV C<br>**GDSM 1:** global increment of RANSE solution |
| Local | Sec. IV B<br>**LKSM 1:** local base flow gradient<br>**LKSM 2:** single period base flow POD | Sec. IV D<br>**LDSM 1:** linearized NSE field at base flow<br>**LDSM 2:** local increment of RANSE solution |

mode deformation are *far smaller* than the severe qualitative distortions that result from ignoring mean field variations.

In summary, the suppression of mean field variations is identified as the dominant cause of inaccurate predictions of the instantaneous growth rate during the natural transient in our benchmark system. A least-order model that employs a fixed base flow will lead to the dramatic mispredictions suggested by the analysis in Sec. III B. Extreme examples of wrong predictions include $\mathcal{P}<0$, hence stability near the steady solution, and $\mathcal{P}\gg 0$, hence strong TKE growth over the natural attractor. The quantitative evaluation of the supplied power also demonstrates that the simple, global kinematic shift mode of Eq. (14) suffices to provide a good estimate of the dynamic contribution of mean field variations.

In the next two sections we shall discuss alternative empirical and analytical definitions of Galerkin approximations of local and global mean field variations. The similarity of the exact dynamic contribution of the mean field, with the estimate obtained with the crudest estimate, will justify the use of the latter, while the finer, analytic definitions are useful to tie this estimate with the analytic justification in Sec. III B.

The results of this section also highlighted, as a secondary effect, the impact of both the truncated energy cascade, and the often ignored effect of transient mode deformation in the Galerkin approximation of $\mathbf{u}'$. As mentioned earlier, the latter effect deserves an independent discussion. It was reviewed and illustrated in[34,49,75] and will be further elaborated in the context of feedback flow control, in a forthcoming article.

## IV. SHIFT MODE DEFINITIONS

Building on the discussion in Sec. III, we now review several methods to estimate modes representing the dynamic mean field correction. In Secs. IV A and IV B, we discuss kinematic definitions based on empirical data. In Secs. IV C and IV D, we elaborate concepts based on dynamic considerations. In each case, we discuss both global and local mean field correction modes. Here, the global versions link the end-points of the natural or forced transient, i.e., steady and periodic solution, while the local cousins refer to short-term changes along that transient. Table I provides a distilled summary of these definitions. Quantitative comparisons of the alternative concepts outlined in this section will be presented in Sec. V. The empirical data used for these definitions and comparisons comprise the two transient simulation trajectories described in Sec. II B.

### A. Global kinematic shift modes (GKSMs)

Here we list two data driven definitions of a single, global mode, aimed to capture the orientation of mean field corrections throughout, along both natural and controlled attractors.

#### *1. GKSM 1: Geometric global correction*

We start with the original definition, as introduced in Ref. 17 and reviewed in Sec. III A

$$\mathbf{u}_\Delta := (\mathbf{u}_0 - \mathbf{u}_s)/\|\mathbf{u}_0 - \mathbf{u}_s\|_\Omega,$$

where $\mathbf{u}_0$ is the mean of the attractor and $\mathbf{u}_s$ is the unstable steady solution. The title *geometric* is due to the fact that this shift mode resolves the missing global direction of the mean field correction along the entire natural transient. Figure 8 depicts $\mathbf{u}_s$, $\mathbf{u}_0$, and the shift mode $\mathbf{u}_\Delta$ as the normalized difference between them. Here and throughout, flow structures are represented by streamlines.

#### *2. GKSM 2: POD-based global correction*

Having extracted the base flow component from the entire data trajectory, as discussed in Sec. II C, POD analysis yields a Galerkin approximation of the base flow

$$\mathbf{u}^B(\mathbf{x},t) = \mathbf{u}_0^B(\mathbf{x}) + \sum_{i=1}^{N_B} a_i^B(t)\mathbf{u}_i^B(\mathbf{x}). \tag{30}$$

Here $\mathbf{u}_0^B$ is the simulation mean and $\{\mathbf{u}_i^B\}_{i=1}^{N_B}$ is a POD basis for $\mathbf{u}^B(\mathbf{x},t)-\mathbf{u}_0^B(\mathbf{x})$. The first and dominant of those modes, $\mathbf{u}_1^B$, is a natural candidate for a kinematic global shift mode, in the sense that it dominates the base flow variations around $\mathbf{u}_0^B$.

This construction is illustrated by Figs. 9 and 10. The former displays the simulation mean and the leading five

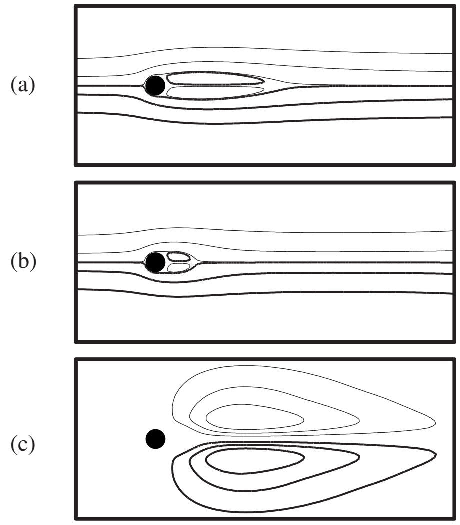


FIG. 8. Construction of the geometric shift mode. (a) The unstable steady solution $\mathbf{u}_s$. (b) The attractor mean flow $\mathbf{u}_0$. (c) The geometric shift mode. According to GKSM 1 this mode is defined as the normalized difference $\mathbf{u}_\Delta := (\mathbf{u}_0 - \mathbf{u}_s)/\|\mathbf{u}_0 - \mathbf{u}_s\|_\Omega$.

POD modes of the natural base flow transient. The latter displays the eigenvalues of the POD correlation matrix, which decline at a near exponential rate, as a function of the mode number, and the time trajectories of the three leading Fourier coefficients. The joint trajectory of the Fourier coefficients is strongly dominated by $a_1$. Indeed, using the dominant POD mode alone, as a single shift mode, provides an average resolution of some 94.5% of the base flow fluctuation energy along the natural transient, and the first three modes provide a near perfect reconstruction with an average of 99% of the entire transient. Furthermore, the leading POD mode is nearly identical to the geometrical definition from Ref. 17, as outlined in GKSM 1. The velocity fields of subsequent eigenmodes (sixth and on, not shown) have the typical structure of second harmonic POD modes, and are therefore attributed primarily to (minor) numerical contamination of the extracted base flow trajectory.

### B. Local kinematic shift modes (LKSMs)

Here we look for modes that resolve the local variations in the base flow, at instantaneous points along natural or actuated transients. We list two alternative definitions.

#### *1. LKSM 1: POD base flow gradient approximation*

Appealing to a local linear approximation

$$\mathbf{u}^B(\mathbf{x},t+\delta t) = \mathbf{u}^B(\mathbf{x},t) + \delta t \cdot \partial_t \mathbf{u}^B(\mathbf{x},t), \tag{31}$$

the normalized gradient $\partial_t \mathbf{u}^B(\mathbf{x},t)/\|\partial_t \mathbf{u}^B(\mathbf{x},t)\|_\Omega$ defines the local orientation of the mean field correction. To alleviate the computational burden and numerical sensitivity of deriving the gradient, we appealed to the global POD representation (30):

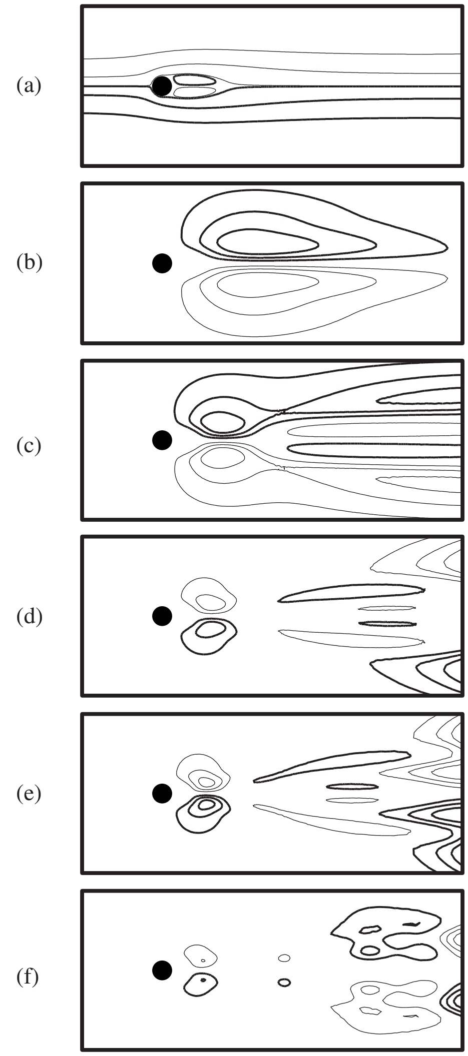


FIG. 9. POD modes of the entire natural base flow transient, as used in definition GKSM 2: the mean of the transient flow is depicted in (a) and the first five POD modes are (b)–(f), all visualized by streamlines. Note that the base flow transient mean (a) is, as expected, an intermediate form between the steady solution and the attractor's mean, depicted in Figs. 8(a) and 8(b). Here and throughout the base flow is computed according to Eq. (5a), using the symmetrized velocity field $\mathbf{u}^{\mathrm{sym}}$.

$$\partial_t \mathbf{u}^B(\mathbf{x},t) = \sum_{i=1}^{N_B} \frac{d}{dt} a_i^B(t)\mathbf{u}_i^B(\mathbf{x}), \tag{32}$$

where $(d/dt)a_i^B$ is locally averaged. Examples of three local shift modes obtained this way are depicted in Fig. 11.

#### *2. LKSM 2: Local POD analysis of base flow increments*

A close variant of LKSM 1 uses a local POD of $\mathbf{u}^B$ over a single period, $\tau \in [t-(T/2), t+(T/2)]$:

$$\mathbf{u}^B(\mathbf{x},\tau) = \mathbf{u}^B(\mathbf{x},t) + \sum_{i=1}^{N_B(t)} a_{t,i}^B(\tau)\mathbf{u}_{t,i}^B(\mathbf{x}). \tag{33}$$

As seen in Figs. 12 and 13, these approximations are each strongly dominated by a single, local shift mode $\mathbf{u}_{t,1}^B$. Comparing Eqs. (33) and (31), the expected similarity, $\mathbf{u}_{t,1}^B \propto \partial_t \mathbf{u}^B(\mathbf{x},t)$, was verified by our numerical data. Shift

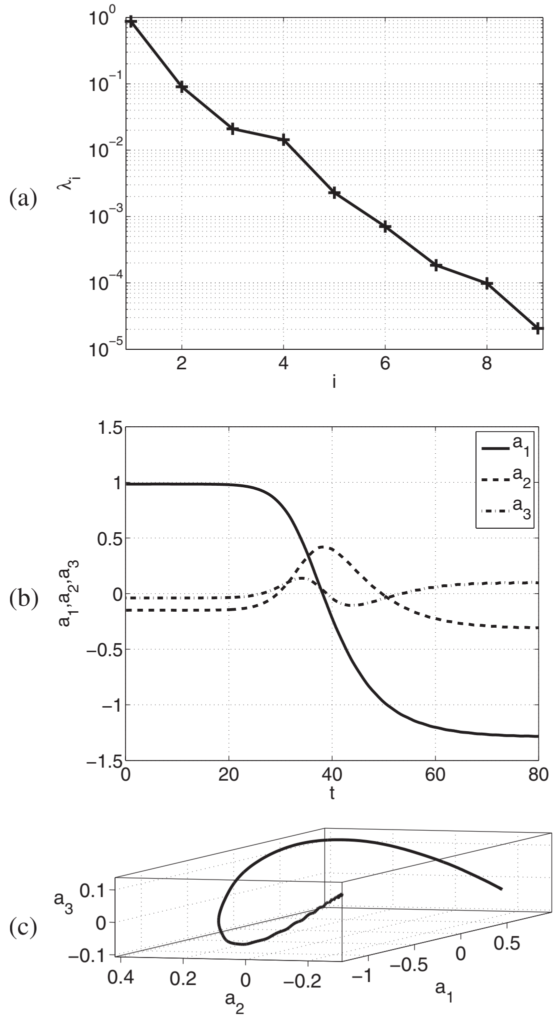


FIG. 10. (a) POD eigenvalues corresponding to Fig. 9, normalized with respect to $\lambda_1$ (i.e., $\lambda_i/\lambda_1$). [(b) and (c)] The trajectories of the corresponding three leading Fourier coefficients.

modes computed by this definition for points along the natural and actuated transient, are shown in Figs. 14 and 15, respectively.

### C. Global dynamic shift mode (GDSM) definition

Here we review shift mode definitions based on dynamic considerations, appealing to the governing NSE. Since, ultimately, these definitions involve numerical computations and empirical data as well, their significance is primarily conceptual, establishing the ties between kinematic observations and first principles.

#### *1. GDSM 1: A Reynolds equation based global shift mode*

This definition parallels GKSM 1, using the RANSE instead of measured data to predict the base flow. An estimate of the attractor mean is produced by solving the RANSE (16a) with the Reynolds stress (16b)

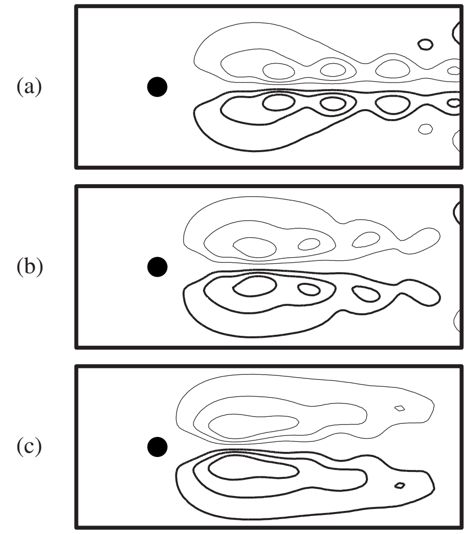


FIG. 11. Kinematic local shift modes obtained according to LKSM 1 as time derivatives of the three-modes POD approximation of the entire natural base flow transients. Henceforth, all local shift modes of the natural and forced transients will be associated both with the mean-period time and with the period-mean TKE. The figures (a)–(c) represent consecutive increments one period apart, with the respective period mean times $t=36$, 41.5, and 46 and TKE levels of 1.17, 2.23, and 2.66 in Fig. 2. The TKE levels will be used to parameterize operating points and compare shift modes obtained at similar TKE levels by the various methods examined here.

$$\nabla \cdot \overline{(\mathbf{u}' \otimes \mathbf{u}')} = \mathcal{K}_* \nabla \cdot (\mathbf{u}_1 \otimes \mathbf{u}_1 + \mathbf{u}_2 \otimes \mathbf{u}_2),$$

where $\mathbf{u}_1$ and $\mathbf{u}_2$ are the attractor's dominant POD modes, and $\mathcal{K}_*$ is the attractor's fluctuation energy. Using the notations of Sec. III B, this means that we substitute $\sqrt{2\mathcal{K}_*}\mathbf{u}_1$ and $\sqrt{2\mathcal{K}_*}\mathbf{u}_2$ for $\mathbf{u}_1^a$ and $\mathbf{u}_1^b$ in Eq. (16b). The steady solution is the RANSE solution corresponding to none of the Reynolds stress. By definition, the attractor mean is the precise RANSE solution when the Reynolds stress is computed in terms of the exact fluctuation. The strong dominance of the attractor's first POD mode pair, representing the first tempo-

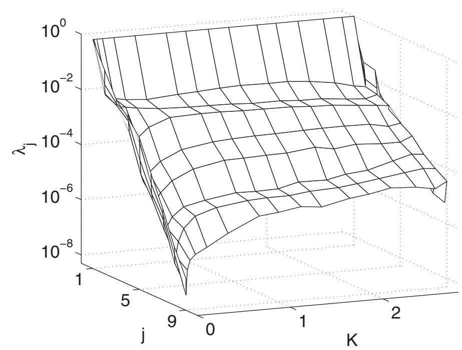


FIG. 12. POD eigenvalues of the natural transient of the base flow $\mathbf{u}^B$ along 20 single periods of the natural transient marked in Fig. 2. The first nine POD eigenvalues of each of the 20 periods, normalized relative to the largest eigenvalue of each periods (i.e., for each period we present $\lambda_j/\lambda_1$). The eigenvalues are plotted as functions of the eigenvalue number $j$ and the mean TKE level $\mathcal{K}$ of the respective period. These are the local kinematic shift modes described in LKSM 2. The increase in significance of $\lambda_j$, $j>1$, near the attractor, is attributed to mean field variations associated with the changes in stability properties during the small, presettling overshoot in $\mathcal{K}$, as seen in Fig. 2.

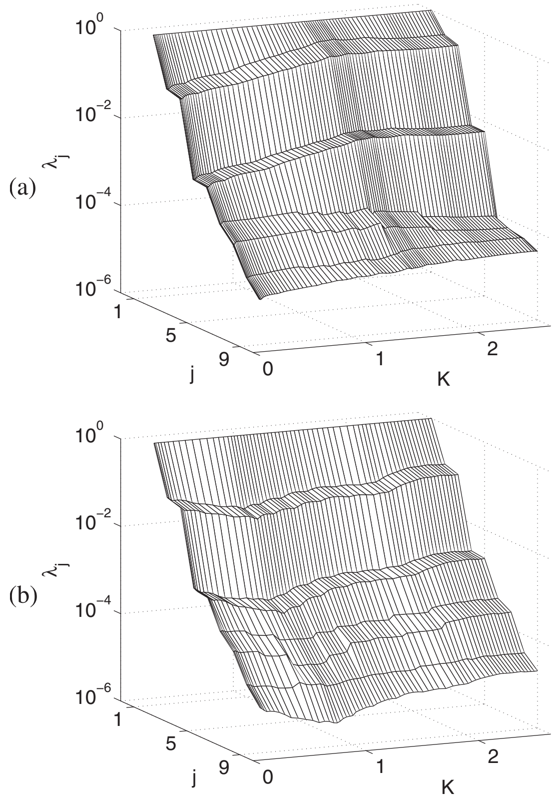


FIG. 13. Counterpart of Fig. 12 for the forced transient: POD eigenvalues of the base flow $\mathbf{u}^B$ along each of 155 single periods of the forced transient, normalized with respect of the dominant eigenvalue (i.e., for each period we present $\lambda_j/\lambda_1$). (a) POD eigenvalues of periods from descending first half of the forced trajectory, from the attractor toward the steady solution. (b) Same, for the ascending second half of the forced trajectory, as it is relaxed from the steady solution to the attractor. Eigenvalues are shown as functions of the eigenvalue number $j$ and that period's TKE level $\mathcal{K}$.

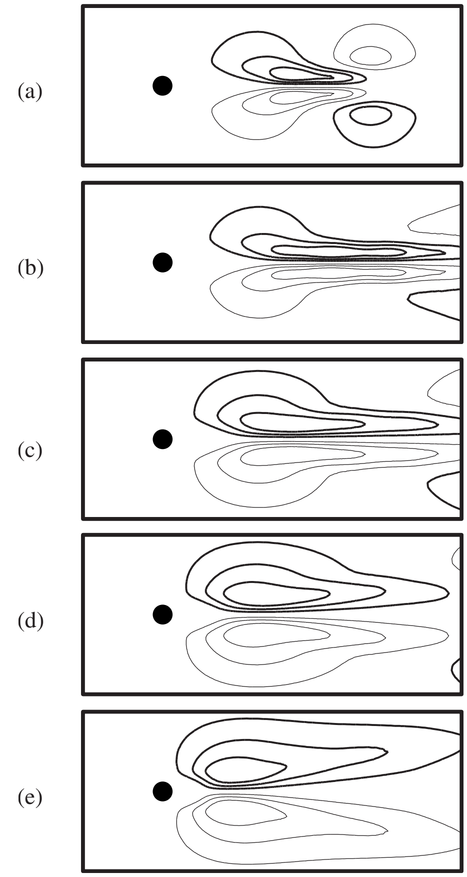


FIG. 14. First POD modes of five selected analyzed periods indicated in Fig. 2 along the natural base flow transient. The respective mean-period times for plots (a)–(e) are $t=16.4$, 26.4, 35, 40.2, and 48.9, and the corresponding period-mean TKE levels are 0.002, 0.1, 1, 1.97, and 2.81.

ral harmonic, translates to a near perfect estimate of the attractor mean. Consequently, the resulting shift mode is essentially identical to the one computed by GKSM 1 and depicted in Fig. 8(c).

### D. Local dynamic shift mode (LDSM) definitions

#### 1. LDSM 1: Linearized corrections from period means

Motivated by Eq. (7), the shift mode is defined as the normalized mean field correction predicted by a linearization at the period mean, $\mathbf{u}^B(\mathbf{x},t)$. An easy approximation is the orientation of the base flow component of a very short simulation, initiated at $\mathbf{u}^B(\mathbf{x},t)$. As will be illustrated in Sec. V, the weakness of this definition is that the Reynolds stress $\nabla\cdot\overline{(\mathbf{u}'\otimes\mathbf{u}')}$ is now missing from Eq. (16a), distorting the predicted correction. Examples of shift modes computed this way are depicted in Fig. 16.

#### 2. LDSM 2: Shift mode based on local increments in solutions of the RANSE

This definition is the one outlined in Sec. III B. The idea is to define $\mathbf{u}_\Delta$ as the orientation of the local increment in RANSE solutions, with the Reynolds stress (16b). The definition in Eq. (16b) is equivalent to

$$\nabla\cdot\overline{(\mathbf{u}'\otimes\mathbf{u}')}=\mathcal{K}\,\nabla\cdot(\mathbf{u}_1\otimes\mathbf{u}_1+\mathbf{u}_2\otimes\mathbf{u}_2),$$

where $\mathcal{K}(t)$ is the mean fluctuation energy over the time window $[t-(T/2),t+(T/2)]$, and $\mathbf{u}_{1,2}$ is the dominant POD mode pair over that window. Examples of shift modes computed this way are depicted in Fig. 17.

## V. QUANTITATIVE COMPARISON

The global shift mode definitions GKSM 1, GKSM 2, and GDSM 1 lead to nearly identical results, rendering further analysis redundant. Quantitative comparisons are thus focused on local shift modes, representing local mean field increments. Comparisons are made in terms of geometrical alignments, as measured by the (absolute value of the) respective inner products. Expectedly, LKSM 1 and LKSM 2 yield essentially identical modes and results are given only for the latter. To make meaningful comparisons between local definitions, especially as we compare the natural and the actuated transients, we parameterize local shift modes by the TKE $\mathcal{K}$ of the operating points at which they are obtained. It is recognized, however, that the TKE parameterization is inevitably method-dependent and thus leads to some mismatched comparisons: in reference to LKSM 2 and LDSM 1, the TKE at the time $t$ is averaged along the respective transient over the period $[t-(T/2),t+(T/2)]$. In reference to

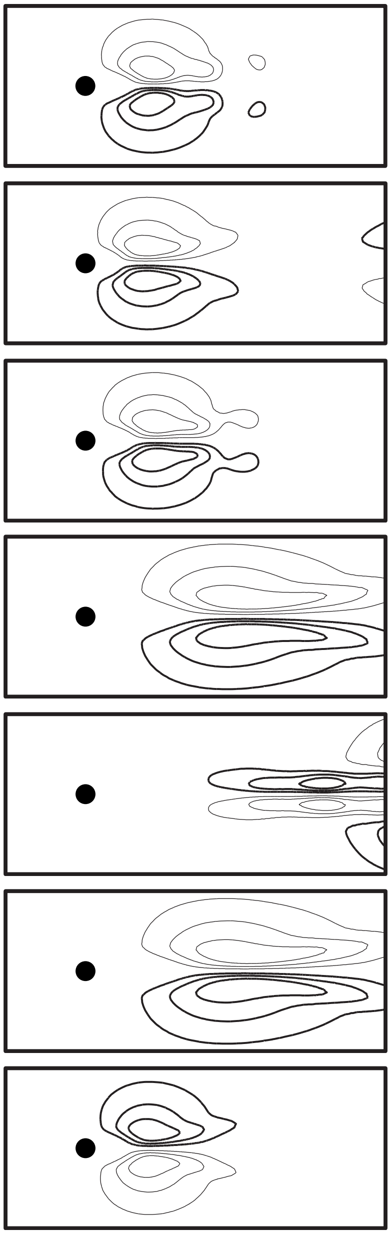


FIG. 15. POD analysis of 155 periods of the actuated transient, as described in Sec. II B. [(a)–(g)] The first (dominant) POD modes of the base flow from seven periods of the actuated transient, computed as in LKSM 2. The respective mean period times are $t=5$, 147.1, 255.1, 399.7, 556.6, 714.2, and 856.4. The corresponding TKE levels read 2.65, 1.9, 1.49, 0.64, 0.18, 1, and 1.8. POD mode streamlines have opposite signs for periods of the descending and ascending trajectories. Quantitative comparisons with other computations in Sec. V take into account the relative proximity to the steady solution or the natural attractor.

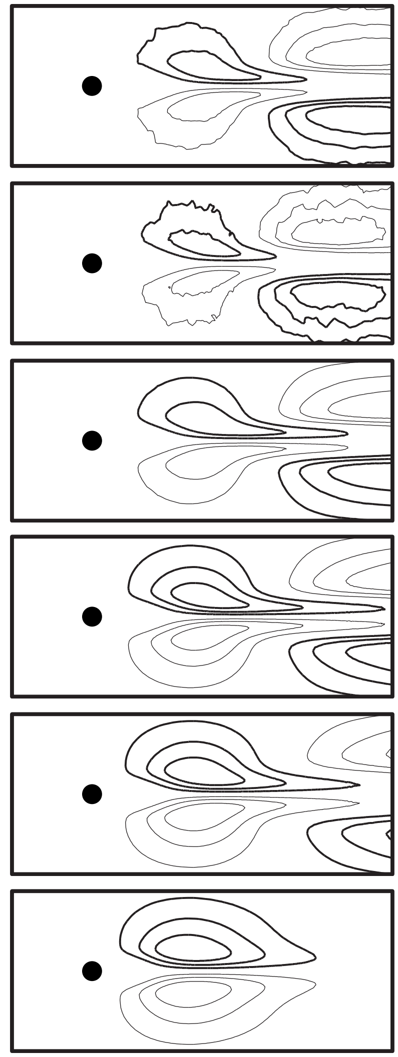


FIG. 16. Six local shift modes computed according to LDSM 1 from short simulations initiated at points along the natural base flow transient. Relating to Fig. 2, plots (a)–(f) correspond to trajectories initiated at $\mathbf{u}^B(\cdot,t)$ with $t=11.5$, 19, 26.5, 34, 39, and 61.4, and approximate TKE levels of 0, 0.06, 0.1, 0.8, 1.78, and 2.69. The clear difference from the LDSM 2 modes in Fig. 17 is explained in the text.

LDSM 2, the operating point is identified by the mean TKE of the two periods that were used in computing the increment in the RANSE solution. The trajectories used are as described in Sec. II B: the natural transient and two parts of a controlled transient, leading from the attractor to the steady solution and then, gradually, back to the attractor. The latter are termed the descending and ascending trajectories, respectively. Correlation matrices are graphically depicted in Figs. 18 and 19 by color code for values in the interval [0,1]. A (quadratic polynomial) line on each of these representations provides a smooth estimate of the crest of the correlation matrix. The main diagonal, marked by a dashed line, provides a reference comparison.

The first comparisons are between the shift modes defined by LKSM 2 for the natural transient and the two parts of the actuated transient. The results are presented in Fig. 18. In interpreting these results, it is necessary to recognize the contribution of the volume force to the base flow, via the Reynolds stress. This contribution can be conceptually partitioned into two components. One is the change of the base flow due to the global attenuation of the fluctuation. The contribution of the attenuated global fluctuation to the Reynolds stress is plausibly comparable to the effect of the fluctuation along the natural transient, at a comparable TKE level. The second component is due to the strong local attenuating impact on the vertical fluctuation in a neighborhood of the volume-force support $\Omega_G$, and thus, on the contribution of that change to the Reynolds stress. The latter is

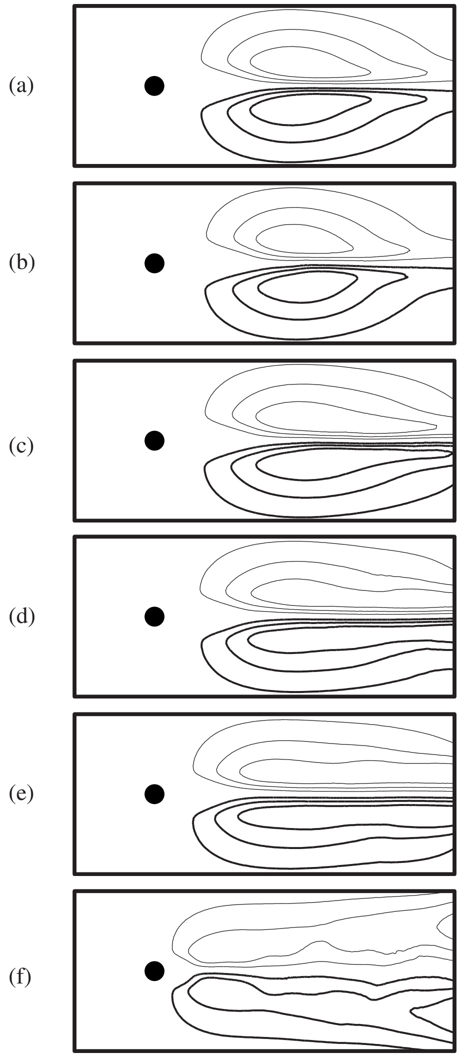


FIG. 17. Six local shift modes computed according to LDSM 2 from evaluation of local increments in RANSE solutions. The respective midperiod times in plots (a)–(f) are the same as the initial times used in the examples in Fig. 16 above; i.e., they are $t=11.5$, 19, 26.5, 34, 39, and 61.4, associated with corresponding approximate TKE levels of 0, 0.06, 0.1, 0.8, 1.78, and 2.69.

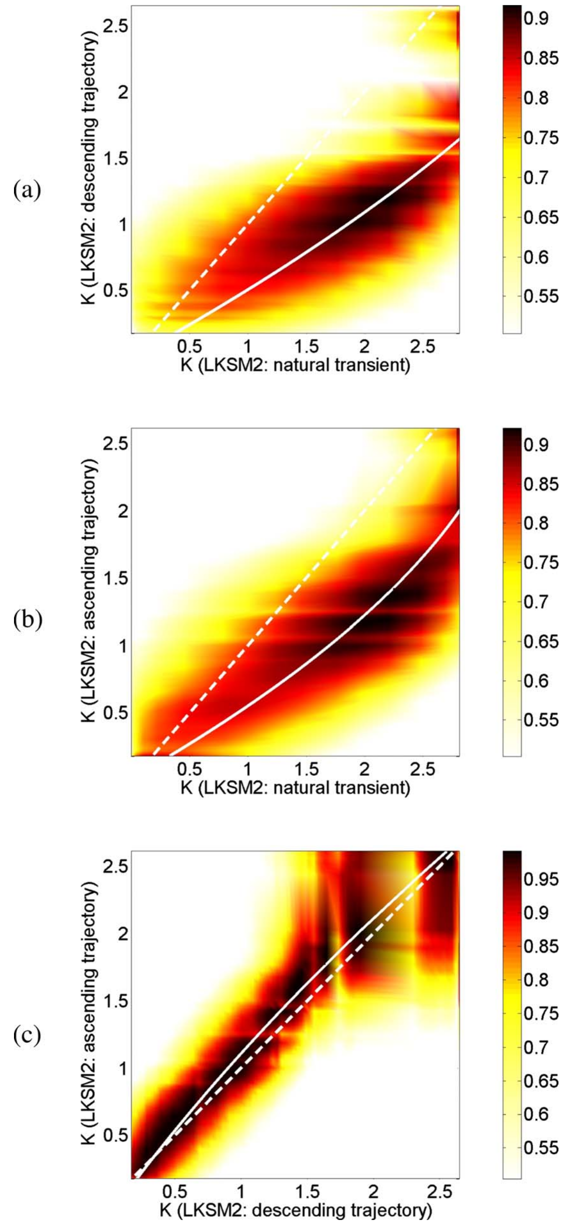


FIG. 18. (Color online) The correlation matrices between different local shift modes computed according to LKSM 2. Color represents the amplitude of the correlation ($\in[0,1]$) between two shift modes. Axes parameterize local shift modes by the associated periods TKE levels. (a) Correlation between shift modes of the natural transient (horizontal axis) and those computed along the descending forced transient (vertical axis). (b) Correlation between shift modes along the natural transient (horizontal axis) and along the ascending forced transient (vertical axis). (c) Correlation between shift modes along the descending forced transient (horizontal axis) and along the ascending forced transient (vertical axis). The solid and dashed white lines indicate the quadratic polynomial approximations of the lines connecting peak values in each row and column of the matrix and the equal TKE levels line, respectively.

most felt near the attractor, where naturally caused changes in the TKE level—and the base flow—over a single period are relatively slow (recall Fig. 2). Indeed, the crest of the correlation between the shift modes associated with the two components of the forced transient nearly coincides with the ideal diagonal, accept for the area departing from, or approaching the attractor. The actuated contribution to the Reynolds stress also explains the fact that local shift modes associated with the natural transient correspond to local shift modes at an otherwise lower levels of fluctuation in the actuated transient. Indeed, this phenomenon is more accentuated in the "descending" actuated trajectory, from the attractor toward the steady solution, where higher actuation levels are employed (again, see Fig. 3), when compared with the "ascending" transient. Nonetheless, considerable similarity is found throughout the TKE range.

Two additional comparisons in Fig. 19 are between the shift modes defined by the kinematic approach of LKSM 2 and the dynamic definitions LDSM 1 and LDSM 2. To avoid the added distortions due to the volume force, we use here only the natural transient.

LDSM 1 represents a near linearization at periods' means. While that is the mean field correction predicted by the reduced order model (7), we noted that it removes the Reynolds stress $\nabla\cdot\overline{(\mathbf{u}'\otimes\mathbf{u}')}$ from the RANSE (16a), anticipating a mismatch with empirical data. Indeed, the peak cor-

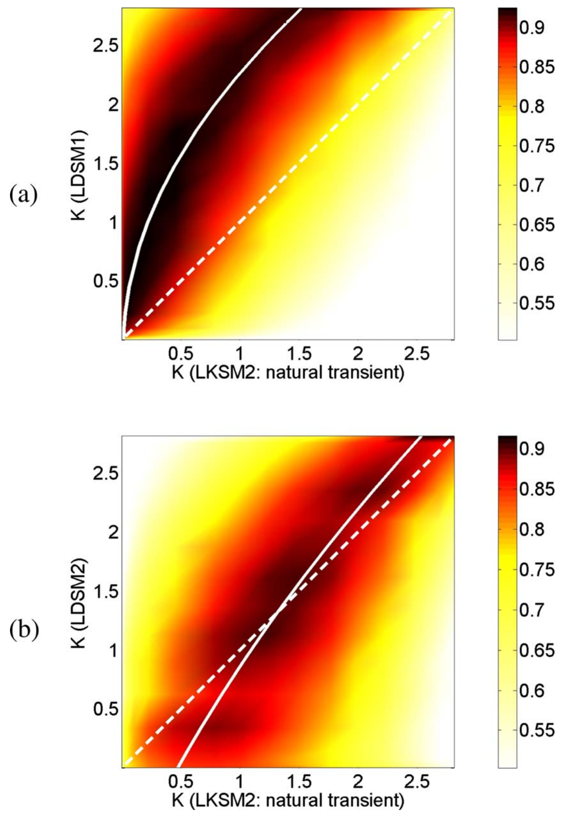


FIG. 19. (Color online) Same as Fig. 18, but for the natural transient, computed by different methods. Color codes, axes parameterizations, and white/dashed white lines are as in Fig. 18. (a) Correlation of shift modes computed according to LKSM 2 (horizontal) and those computed according to LDSM 1 (vertical). (b) Correlation of shift modes computed according to LKSM 2 (horizontal) and those computed according to LDSM 2 (vertical).

relation between empirical shift modes according to LKSM 2 and those obtained with LDSM 1 occurs when the latter is associated with a much higher level of fluctuations. This observation matches an independent observation by the authors concerning the best match between POD modes of natural and controlled attractors, on one hand, and linear stability modes associated with linearizations about the means of attractors, on the other hand: the best match is found when the stability modes are computed for linearization about a period mean associated with considerably higher levels of fluctuations than the period from which the POD modes are extracted.[75]

In contrast, the correlations of the local kinematic shift modes according to LKSM 2 with the shift modes associated with local incremental changes in solutions of the RANSE, according to LDSM 2, crest much closer to the ideal diagonal. The residual mismatch, in this case, might be attributed simply to a combination of the different associations of each shift mode with a TKE level in the two methods and to the suppression of the time derivative in the Reynolds equation in LDSM 2.

The results presented in Figs. 18 and 19 can be summarized with the following observations:

- First and foremost, indeed, the local shift modes obtained a transient trajectory (here, the natural transient) either empirically, by LKSM 2 or by LDSM 2, appealing to first principles, are very similar.
- Second, as predicted by theory, the local shift mode is affected by the contribution of periodic actuation to the Reynolds stress. That effect is determined by the actuation amplitude and is relatively small under low gain actuation.
- Third, theory predicts a mismatch between observed local mean field corrections and the shift modes obtained by the approximate linearization method LDSM 1. Interestingly, similarity is regained if an appropriate shift in the TKE between the respective reference points is used, in agreement with independent observation in Ref. 75, regarding the similarity of linear stability modes and POD modes.

We close this quantitative analysis with a comparison of one local shift mode, empirically obtained according to LKSM 2, with best matching local shift modes obtained by LKSM 2 from the actuated trajectories, and by LDSM 1 and LDSM 2, from the natural trajectory. The selected LKSM 2 mode is extracted from the natural transient at the intermediate point of $\mathcal{K}=1.463$. The modes are depicted in Fig. 20 and the quantitative correlations in Fig. 21. These comparisons illustrate the close similarity of the orientation of mean field corrections across computation methods and even when factoring the effects of actuation on changes in the transient trajectory. In fact, that similarity is maintained even when a simplified version of Reynolds stress incremental modes LDSM 2 is used, whereby instead of representing local fluctuations by local POD modes, scaled versions of the natural attractor POD modes are used throughout.

## VI. CONCLUDING REMARKS

In the first pioneering POD Galerkin model of wall turbulence,[22] mean flow variations were included as an auxiliary stabilizing model by coupling the RANSE with a Galerkin model. This procedure leads to cubic terms in the dynamical system for the mode coefficients.[83] Such a coupling requires a time-scale separation between base flow and fluctuation dynamics, which may be questionable or is at least difficult to achieve.[18]

The introduction of the shift mode as a representation of a missing state-space direction in Ref. 17 created a mathematically rigorous framework for the inclusion of base flow variations in POD models. As illustrated in Ref. 17, the inclusion of mean field dynamics is an essential enabler for transient representation in minimal order models of the attractive inertial manifold, connecting the unstable steady solution and the limit cycle. This role has since been demonstrated in a succession of flow control studies by several groups.

The present article is focused on the dynamic, NSE roots of mean field models. In Sec. III B we elaborated the essential role of the dynamic coupling of mean field corrections and fluctuation growth rates, in terms of the coupling between the RANSE and a harmonic fluctuation equation, obtained by the temporal projection of the NSE at the dominant frequency (or frequency band) of the instability. In these

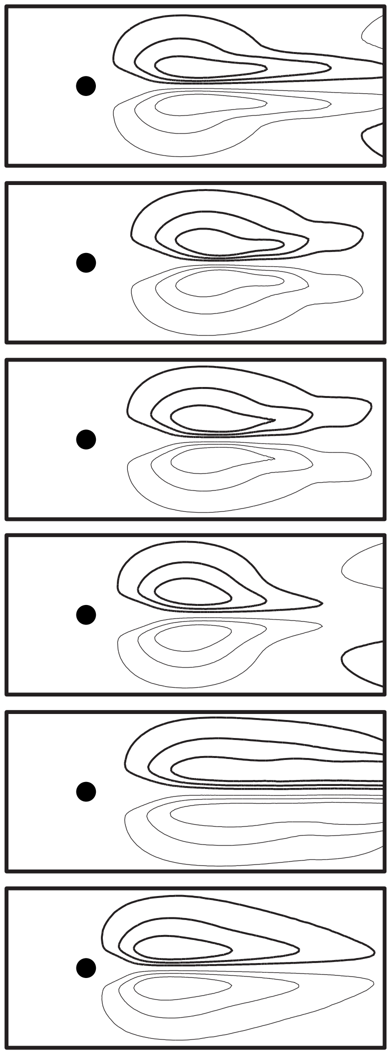


FIG. 20. Plots of the LKSM 2 mode of the natural transient at $\mathcal{K}=1.4638$ (a), followed by the best matches of that modes by LKSM 2 modes from the descending [(b), $\mathcal{K}=0.8537$] and ascending [(c), $\mathcal{K}=0.9668$] actuated transients. Next are the best matches of (a) by local shift modes along the natural transient, computed according to LDSM 1 [(d), $\mathcal{K}=2.6366$] and LDSM 2 [(e), $\mathcal{K}=1.5682$]. The last plot was computed by a simplified version of LDSM 2 [(f), $\mathcal{K}=1.5319$], where the fluctuation is modeled by the dominant POD mode pair of the attractor, scaled by the local TKE, instead of by the POD mode pair of the transient period under consideration.

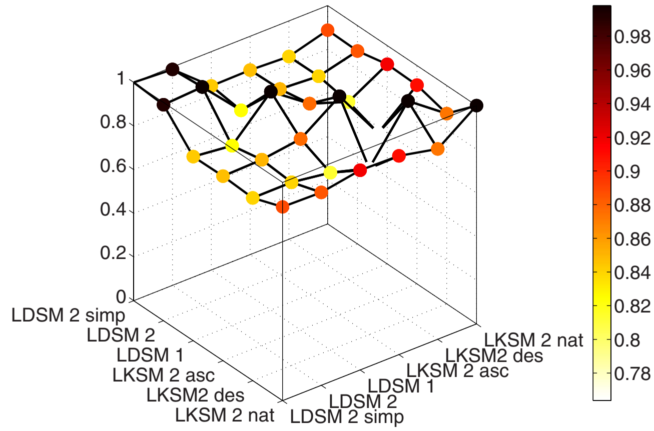


FIG. 21. (Color online) Correlations of the best matching shift modes in Fig. 20. Labels indicate the LKSM 2 mode of the natural transient (LKSM 2 natural), and the best matches with LKSM 2 modes from the descending and ascending actuated trajectories (LKSM 2 descending and LKSM 2 ascending, respectively), the shift modes obtained from the natural transient according to LDSM 1, LDSM 2, and the simplified version of the latter (LDSM 2 simple), where the scaled attractor POD modes where used instead of the local POD modes, used in LDSM 2.

terms, the equation governing the amplitude of a shift mode is viewed as a Galerkin system counterpart of the RANSE, and the need to include that equation in the Galerkin model is tied to the essential role of the bilateral coupling between the mean field and the fluctuation, in the NSE. The analysis in Sec. III B also reveals the local form of a shift mode, defined as the tangent direction of local mean field corrections.

A detailed examination of the transient modal energy flow in the cylinder wake flow benchmark was introduced in Sec. III C as a new tool to quantitatively evaluate the dynamic role of individual modes. It was used to illustrate and validate the formal analysis in Sec. III B. Indeed, that analysis demonstrates that the suppression of mean field variations is the dominant cause of dynamic distortions in least-order Galerkin representations. Depending on the selected combination of a fixed base flow and of modes representing the periodic fluctuation, such distortions can be extreme. Indeed, they can lead to predictions that are directly contrary to basic qualitative properties of the flow. Examples include the predictions of TKE decay near the steady solution, and of fast TKE growth, in the vicinity of the actual attractor, i.e., in both cases the prediction is the very opposite of the actual transient behavior. In contrast, the inclusion of even the simplest mean field representation, rectifies such distortions, complementing the observations in Ref. 17 and in subsequent studies. Transient modal energy flow analysis highlighted additional important, albeit secondary sources of dynamic distortions in standard POD models. Those include the truncation of the energy cascade and the dynamic deformation along transients of coherent structures that dominate the periodic fluctuation.

The article continues with an exploration and refinement of a set of natural shift mode definitions, in Sec. IV, based on analytic-dynamic and geometric-kinematic definitions of shift modes, as the orientations of local and global mean field corrections. The quantitative comparisons of these definitions in Sec. V reveal the consistency of the mean field correction: in a nutshell, the shift mode is no accident; rather, it is an intrinsic and critical player in system dynamics. Our analysis also reveals that, much like the deformation of dominant fluctuation modes,[34,49,75] the shift mode is subject to slow deformation as the system transitions between operating conditions.

The observation that the simplest and easiest to compute global kinematic shift mode produced a decent approximation of the dynamic impact of the exact mean field was made in Sec. III C, based on quantitative power flow analysis. That key observation adds a dynamic perspective to the comparisons in Sec. V, while the analytical definitions provide the conceptual bridge to the NSE, the simple kinematic definition is established as an ample, convenient, and easily computable modeling option.

For other flows, however, local shift modes may be needed to account more accurately for mean field deformations through the integration of local increments. The discussion in Ref. 34 is a case in point. As elaborated in the Appendix, an effective feedback policy needs to determine the control input so that $\mathcal{P}_a$, in Eq. (18), will be close to balancing the natural flow components of $\mathcal{P}$, which requires a precise estimate of the local mean field. Once again, however, the conceptual inclusion of local mean field deformations in the Galerkin model does not translate to intractable complexity of control design. To see this point one needs to distinguish between the role of the Galerkin model as an encapsulation of the pertinent fundamentals of the flow, guiding controller structure, and controller realization. The controller itself can often be realized in terms of far simpler and more robust combinations of moderately nonlinear filters/adaptors, and static nonlinearities. That is precisely the case in Ref. 34, which is focused on the need to account for the transient deformation of dominant coherent structures.

## ACKNOWLEDGMENTS

The authors gratefully acknowledge funding from the U.S. National Science Foundation (NSF) under Grant Nos. 0524070 and 0410246, from the U.S. Air Force Office of Scientific Research (AFOSR) under Grant Nos. FA9550-0610373 and FA9550-0510399, and from the Deutsche Forschungsgemeinschaft (DFG) under Grant Nos. 258/1-1 and 258/2-3 and via the Collaborative Research Center (Grant No. Sfb 557) "Control of Complex Turbulent Shear Flows" at the Berlin Institute of Technology, and from CNRS, e.g., via Invited Researcher grants. The authors acknowledge stimulating discussions with Katarina Aleksic, Laurent Cordier, Mark Luchtenburg, Rudibert King, Mark Pastoor, Michael Schlegel, Jon Scouten, Stefan Siegel, Tino Weinkauf, and Jose-Eduardo Wesfreid. We are grateful for outstanding hardware and software support by Lars Oergel and Martin Franke at the Berlin Institute of Technology. Finally, we wish to thank two anonymous referees for very insightful comments.

## APPENDIX: DISSIPATIVE FEEDBACK CONTROL

This appendix reviews the control that yielded the actuated data in Fig. 3 and elucidates the essential role of mean field variations in feedback flow control.

Let the energy flow equation (17) be abbreviated as

$$\frac{d}{dt}\mathcal{K} = \mathcal{P} = \mathcal{P}_n + \mathcal{P}_a,$$

where $\mathcal{P}_n$ is the natural power component. In these terms, a control command is dissipative when

$$\mathcal{P}_a = (\mathbf{f},\mathbf{u})_\Omega = G(\mathbf{g},\mathbf{u})_\Omega < 0. \tag{A1}$$

Invoking Eq. (22), we can write

$$(\mathbf{g},\mathbf{u}(\cdot,t))_\Omega = \sqrt{\mathcal{K}}r_g(\mathbf{u}^a,\mathbf{u}^b)\cos[\omega(\epsilon t)t + \phi(\epsilon t)].$$

where $r_g(\epsilon t) > 0$ is slowly varying. Under Sec. III B 1 a, the control command is a sinusoidal of the form (19). In particular, dissipativity requires

$$G(t) = -\tilde{G}(t)\cos[\omega(\epsilon t)t + \phi(\epsilon t)], \quad \tilde{G} > 0. \tag{A2}$$

This leads to the period average of $\overline{\mathcal{P}}_a = -(1/2)\tilde{G}\sqrt{\mathcal{K}}r_g$.

A complete information control does not restrict actuation levels, as long as Eq. (A1) is satisfied. Sensor feedback, however, must maintain the model's validity envelope,[29,53] restricting actuation to

$$\tfrac{1}{2}\tilde{G}\sqrt{\mathcal{K}}r_g = -\mathcal{P}_a = \mathcal{P}_n \pm \epsilon \Leftrightarrow \mathcal{P} = \pm \epsilon, \tag{A3}$$

where $\epsilon > 0$ is small relative to $\mathcal{P}_n$.

Conditions (A2) and (A3) are universal in the sense that any realistic, model-based stabilizing sensor feedback, using essentially any actuation, must be both nearly periodic and slowly dissipate period-averaged TKE. Two conclusions from these observations are that the data in Fig. 3, which was generated under these constraints, is generic, and that an exact account for the reflection of base flow variations in the value of $\mathcal{P}_n$ is vital for feedback wake attenuation.

The significance of a low order Galerkin model is precisely in exposing and encapsulating these conditions. Feedback realization can actually be much simpler[34] (see also Ref. 88), and include a moderately nonlinear filter that estimates the operating point and oscillation phase, and a static nonlinearity that translates the estimate of the operating point to the balancing value of $\tilde{G}$.

[1]K. Karhunen, "Über lineare Methoden in der Wahrscheinlichkeitsrechnung," Ann. Acad. Sci., Fenn., Ser. A1: Math.-Phys. **37**, 1 (1946).
[2]M. M. Loève, *Probability Theory* (Van Nostrand, Princeton, 1955).
[3]E. N. Lorenz, "Empirical orthogonal functions and statistical weather prediction," Scientific Report No. 1, Statistical Forecasting Project, Department of Meteorology, Massachusetts Institute of Technology, Boston, 1956.
[4]V. R. Algazi and D. J. Sakrison, "On the optimality of the Karhunen–Loève expansion," IEEE Trans. Inf. Theory **15**, 319 (1969).
[5]L. Sirovich, "Turbulence and the dynamics of coherent structures, Part I: Coherent structures; Part II: Symmetries and transformations; Part III: Dynamics and scaling," Q. Appl. Math. **45**, 561 (1987).
[6]P. Holmes, J. L. Lumley, and G. Berkooz, *Turbulence, Coherent Structures, Dynamical Systems and Symmetry* (Cambridge University, Cambridge, 1998).
[7]T. R. Smith, J. Moehlis, and P. Holmes, "Low-dimensional modelling of turbulence using the proper orthogonal decomposition: A tutorial," Nonlinear Dyn. **41**, 275 (2005).
[8]C. P. Jackson, "A finite-element study of the onset of vortex shedding in flow past variously shaped bodies," J. Fluid Mech. **182**, 23 (1987).
[9]A. Zebib, "Stability of viscous flow past a circular cylinder," J. Eng. Math. **21**, 155 (1987).
[10]E. Åkervik, J. Hœpffner, U. Ehrenstein, and D. S. Henningson, "Optimal growth, model reduction and control in a separated boundary-layer flow using global eigenmodes," J. Fluid Mech. **579**, 305 (2007).
[11]M. Chevalier, J. Hœpffner, E. Åkervik, and D. S. Henningson, "Linear feedback control and estimation applied to instabilities in spatially developing boundary layers," J. Fluid Mech. **588**, 163 (2007).
[12]S. Lall, J. E. Marsden, and S. Glavaski, "A subspace approach to balanced truncation for model reduction of nonlinear control systems," Int. J. Robust Nonlinear Control **12**, 519 (2002).

[13]K. Willcox and J. Peraire, "Balanced model reduction via the proper orthogonal decomposition," AIAA J. **40**, 2323 (2002).
[14]C. W. Rowley, "Model reduction for fluids, using balanced proper orthogonal decomposition," Int. J. Bifurcation Chaos **15**, 997 (2005).
[15]Z. Ma, C. W. Rowley, and G. Tadmor, "Snapshot-based balanced truncation for linear time-periodic systems," IEEE Trans. Autom. Control **55**, 469 (2010).
[16]A. E. Deane, I. G. Kevrekidis, G. E. Karniadakis, and S. A. Orszag, "Low-dimensional models for complex geometry flows: Application to grooved channels and circular cylinders," Phys. Fluids A **3**, 2337 (1991).
[17]B. R. Noack, K. Afanasiev, M. Morzyński, G. Tadmor, and F. Thiele, "A hierarchy of low-dimensional models for the transient and post-transient cylinder wake," J. Fluid Mech. **497**, 335 (2003).
[18]D. Rempfer, "Empirische Eigenfunktionen und Galerkin-Projektionen zur Beschreibung des laminar-turbulenten Grenzschichtumschlags (transl.: Empirical eigenfunctions and Galerkin projection for the description of the laminar-turbulent boundary-layer transition)," Habilitation thesis, Fakultät für Luft- und Raumfahrttechnik, Universität Stuttgart, 1995.
[19]D. Rempfer, "On low-dimensional Galerkin models for fluid flow," Theor. Comput. Fluid Dyn. **14**, 75 (2000).
[20]C. Foias, G. R. Sell, and R. Temam, "Inertial manifolds for nonlinear evolutionary equations," J. Differ. Equations **73**, 309 (1988).
[21]S. Ahuja, C. W. Rowley, I. G. Kevrekidis, M. Wei, T. Colonius, and G. Tadmor, "Low-dimensional models for control of leading-edge vortices: Equilibria and linearized models," Proceedings of the 45th AIAA Aerospace Sciences Meeting and Exhibit, 2007, AIAA Paper 2007-0709.
[22]N. Aubry, P. Holmes, J. L. Lumley, and E. Stone, "The dynamics of coherent structures in the wall region of a turbulent boundary layer," J. Fluid Mech. **192**, 115 (1988).
[23]J. T. Stuart, "On the non-linear mechanics of hydrodynamic stability," J. Fluid Mech. **4**, 1 (1958).
[24]J. T. Stuart, "Nonlinear stability theory," Annu. Rev. Fluid Mech. **3**, 347 (1971).
[25]J. Dušek, P. Le Gal, and P. Fraunie, "A numerical and theoretical study of the first Hopf bifurcation in a cylinder wake," J. Fluid Mech. **264**, 59 (1994).
[26]B. J. A. Zielinska and J. E. Wesfreid, "On the spatial structure of global modes in the wake flow," Phys. Fluids **7**, 1418 (1995).
[27]J. E. Wesfreid, S. Goujon-Durand, and B. J. A. Zielinska, "Global mode behavior of the streamwise velocity in wakes," J. Phys. II **6**, 1343 (1996).
[28]B. J. A. Zielinska, S. Goujon-Durand, J. Dušek, and J. E. Wesfreid, "Strongly nonlinear effect in unstable wakes," Phys. Rev. Lett. **79**, 3893 (1997).
[29]J. Gerhard, M. Pastoor, R. King, B. R. Noack, A. Dillmann, M. Morzyński, and G. Tadmor, "Model-based control of vortex shedding using low-dimensional Galerkin models," Proceedings of the 33rd AIAA Fluids Conference and Exhibit, 2003, AIAA Paper 2003-4262.
[30]S. Siegel, K. Cohen, and T. McLaughlin, "Feedback control of a circular cylinder wake in experiment and simulation," Proceedings of the 33rd AIAA Fluids Conference and Exhibit, 2003, AIAA Paper 2003-3571.
[31]S. Siegel, K. Cohen, and T. McLaughlin, "Experimental variable gain feedback control of a circular cylinder wake," Proceedings of the 24th AIAA Aerodynamic Measurement Technology and Ground Testing Conference, 2004, AIAA Paper 2004-2611.
[32]G. Tadmor, B. R. Noack, M. Morzyński, and S. Siegel, "Low-dimensional models for feedback flow control. Part II: Controller design and dynamic estimation," Proceedings of the 2nd AIAA Flow Control Conference, 2004, AIAA Paper 2004-2409.
[33]B. R. Noack, G. Tadmor, and M. Morzyński, "Low-dimensional models for feedback flow control. Part I: Empirical Galerkin models," Proceedings of the 2nd AIAA Flow Control Conference, 2004, AIAA Paper 2004-2408.
[34]O. Lehmann, M. Luchtenburg, B. R. Noack, R. King, M. Morzynski, and G. Tadmor, "Wake stabilization using POD Galerkin models with interpolated modes," Proceedings of 44th IEEE Conference on Decision and Control and European Control Conference ECC, Seville, Spain, 2005, p. 500.
[35]S. Siegel, J. Seidel, C. Fagley, M. Luchtenburg, K. Cohen, and T. McLaughlin, "Low-dimensional modelling of a transient cylinder wake using double proper orthogonal decomposition," J. Fluid Mech. **610**, 1 (2008).
[36]M. Luchtenburg, B. R. Noack, B. Günther, R. King, and G. Tadmor, "A generalised mean-field model of the natural and high-frequency actuated flow around a high-lift configuration," J. Fluid Mech. **623**, 283 (2009).
[37]O. Marquet, D. Sipp, and L. Jacquin, "Sensitivity analysis and passive control of cylinder flow," J. Fluid Mech. **615**, 221 (2008).
[38]B. Thiria and J. E. Wesfreid, "Stability properties of forced wakes," J. Fluid Mech. **579**, 137 (2007).
[39]B. Protas and A. Styczek, "Optimal rotary control of the cylinder wake in the laminar regime," Phys. Fluids **14**, 2073 (2002).
[40]B. Protas and J. E. Wesfreid, "Drag force in the open-loop control of the cylinder wake in the laminar regime," Phys. Fluids **14**, 810 (2002).
[41]L. D. Landau and E. M. Lifshitz, *Fluid Mechanics (Course of Theoretical Physics)* (Pergamon, Oxford, 1987), Vol. 6.
[42]K. R. Sreenivasan, P. J. Strykowski, and D. J. Olinger, "Hopf bifurcation, Landau equation, and vortex shedding behind circular cylinders," in *Forum on Unsteady Flow Separation*, edited by K. N. Ghia (American Society for Mechanical Engineers, Fluids Engineering Division, New York, 1987), Vol. 52, pp. 1–13.
[43]M. C. Thompson and P. Le Gal, "The Stuart–Landau model applied to wake transition revisited," Eur. J. Mech. B/Fluids **23**, 219 (2004).
[44]M. Morzyński, K. Afanasiev, and F. Thiele, "Solution of the eigenvalue problems resulting from global non-parallel flow stability analysis," Comput. Methods Appl. Mech. Eng. **169**, 161 (1999).
[45]G. E. Karniadakis and G. S. Triantafyllou, "Three-dimensional dynamics and transition to turbulence in the wake of bluff bodies," J. Fluid Mech. **238**, 1 (1992).
[46]B. R. Noack and H. Eckelmann, "A global stability analysis of the steady and periodic cylinder wake," J. Fluid Mech. **270**, 297 (1994).
[47]H.-Q. Zhang, U. Fey, B. R. Noack, M. König, and H. Eckelmann, "On the transition of the cylinder wake," Phys. Fluids **7**, 779 (1995).
[48]D. Barkley and R. D. Henderson, "Three-dimensional floquet stability analysis of the wake of a circular cylinder," J. Fluid Mech. **322**, 215 (1996).
[49]M. Morzyński, B. R. Noack, and G. Tadmor, "Global flow stability analysis and reduced order modeling for bluff-body flow control," Theor Appl. Mech. **45**, 621 (2007).
[50]M. F. Unal and D. Rockwell, "On the vortex formation from a cylinder; Part 2. Control by a splitter-plate interference," J. Fluid Mech. **190**, 513 (1988).
[51]P. J. Strykowski and K. R. Sreenivasan, "On the formation and suppression of vortex shedding at low Reynolds numbers," J. Fluid Mech. **218**, 71 (1990).
[52]E. Detemple-Laake and H. Eckelmann, "Phenomenology of Kármán vortex streets in oscillatory flow," Exp. Fluids **7**, 217 (1989).
[53]K. Roussopoulos, "Feedback control of vortex shedding at low Reynolds numbers," J. Fluid Mech. **248**, 267 (1993).
[54]K. Roussopoulos and P. A. Monkewitz, "Nonlinear modelling of vortex shedding control in cylinder wakes," Physica D **97**, 264 (1996).
[55]M. Bergmann, L. Cordier, and J.-P. Brancher, "Optimal rotary control of the cylinder wake using proper orthogonal decomposition reduced order model," Phys. Fluids **17**, 097101 (2005).
[56]B. H. Kim and D. R. Williams, "Nonlinear coupling of fluctuating drag and lift on cylinders undergoing forced oscillations," J. Fluid Mech. **559**, 335 (2006).
[57]B. Protas, "Linear feedback stabilization of laminar vortex shedding based on a point vortex model," Phys. Fluids **16**, 4473 (2004).
[58]B. R. Noack, G. Tadmor, and M. Morzyński, "Actuation models and dissipative control in empirical Galerkin models of fluid flows," Proceedings of the 2004 American Control Conference, 2004, Vol. 6, p. 5722.
[59]G. C. Lewin and H. Haj-Hariri, "Reduced-order modeling of a heaving airfoil," AIAA J. **43**, 270 (2005).
[60]S. M. Djouadi, R. C. Camphouse, and J. H. Myatt, "Reduced order models for boundary feedback flow control," Proceedings of the 2008 American Control Conference, 2008, p. 4005.
[61]R. D. Wallace, M. Y. Andino, M. N. Glauser, R. C. Camphouse, R. F. Schmit, and J. H. Myatt, "Flow and aero-optics around a turret Part 2: Surface pressure based proportional closed loop flow control," Proceedings of the 39th AIAA Plasmadynamics and Lasers Conference, 2008, AIAA Paper 2008-4217.
[62]S. Ahuja and C. W. Rowley, "Low-dimensional models for feedback stabilization of unstable steady states," Proceedings of the 46th AIAA Aerospace Sciences Meeting and Exhibit, 2008, AIAA Paper 2008-553.
[63]G. K. Batchelor, *An Introduction to Fluid Dynamics*, Mathematical Library Series (Cambridge University Press, Cambridge, 2000).
[64]W. Stankiewicz, M. Morzyński, B. R. Noack, and G. Tadmor, "Reduced order Galerkin model of flow around a NACA-0012 airfoil," Math. Modell. Anal. **13**, 113 (2008).

[65] G. Tadmor, M. D. Centuori, B. R. Noack, M. Luchtenburg, O. Lehmann, and M. Morzyński, "Low order Galerkin models for the actuated flow around 2-D airfoils," Proceedings of the 45th AIAA Aerospace Sciences Meeting and Exhibit, 2007, AIAA Paper 2007-1313.

[66] S. Raghu and P. A. Monkewitz, "The bifurcation of a hot round jet to limit-cycle oscillations," Phys. Fluids A **3**, 501 (1991).

[67] F. Li, G. Tadmor, A. Banaszuk, B. R. Noack, and P. G. Mehta, "A reduced order Galerkin model for the reacting flameholder," Proceedings of the 3rd AIAA Flow Control Conference, 2006, AIAA Paper 2006-3487.

[68] M. Farhood, C. L. Beck, and G. E. Dullerud, "Model reduction of periodic systems: A lifting approach," Automatica **41**, 1085 (2005).

[69] V. B. Kolmanovskii, *Stability and Periodic Solutions of Controlled Systems with Delay* (Nauka, Moscow, 1981).

[70] B. Bamieh, J. B. Pearson, B. A. Francis, and A. Tannenbaum, "A lifting technique for linear systems with applications to sampled-data control," Syst. Control Lett. **17**, 79 (1991).

[71] G. Tadmor, "$H_\infty$ optimal sampled data control in continuous time systems," Int. J. Control **56**, 99 (1992).

[72] B. R. Noack, P. Papas, and P. A. Monkewitz, "Low-dimensional Galerkin model of a laminar shear-layer," Technical Report No. 2002-01, Laboratoire de Mécanique des Fluides, Département de Genie Mécanique, Ecole Polytechnique Fédérale de Lausanne, Switzerland, 2002.

[73] B. R. Noack, P. Papas, and P. A. Monkewitz, "The need for a pressure-term representation in empirical Galerkin models of incompressible shear flows," J. Fluid Mech. **523**, 339 (2005).

[74] X. Ma and G. E. Karniadakis, "A low-dimensional model for simulating three-dimensional cylinder flow," J. Fluid Mech. **458**, 181 (2002).

[75] M. Morzyński, W. Stankiewicz, B. R. Noack, R. King, F. Thiele, and G. Tadmor, "Continuous mode interpolation for control-oriented models of fluid flow," in *Active Flow Control*, Notes on Numerical Fluid Mechanics and Multidisciplinary Design Vol. 95, edited by R. King (Springer-Verlag, Berlin, 2007), pp. 260–278.

[76] W. L. IJzerman, "Signal representation and modeling of spatial structures in fluids," Ph.D. thesis, Universiteit Twente, 2000.

[77] J. Borggaard, A. Hay, and D. Pelletier, "Interval-based reduced order models for unsteady fluid flow," IJNAM **4**, 353 (2007).

[78] A. Hay, J. Borggaard, and D. Pelletier, "Local improvements to reduced-order models using sensitivity analysis of the proper orthogonal decomposition," J. Fluid Mech. **629**, 41 (2009).

[79] D. Barkley, "Linear analysis of the cylinder wake mean flow," Europhys. Lett. **75**, 750 (2006).

[80] B. R. Noack, M. Schlegel, B. Ahlborn, G. Mutschke, M. Morzyński, P. Comte, and G. Tadmor, "A finite-time thermodynamics of unsteady flows," J. Non-Equilib. Thermodyn. **33**, 103 (2008).

[81] B. R. Noack, M. Schlegel, M. Morzyński, and G. Tadmor, "System reduction strategy for Galerkin models of fluid flows," Int. J. Numer. Methods Fluids (in press).

[82] D. Rempfer, "Kohärente Strukturen und Chaos beim laminar-turbulenten Grenzschichtumschlag (transl.: Coherent structures and chaos of the laminar-turbulent boundary-layer transition)," Ph.D. thesis, Fakultät Verfahrenstechnik der Universität Stuttgart, 1991. [Part of this work has been published in the following papers: D. Rempfer and H. F. Fasel, "Evolution of three-dimensional coherent structures in a flat-plate boundary layer," J. Fluid Mech. **260**, 351 (1994); "Dynamics of three-dimensional coherent structures in a flat-plate boundary layer," *ibid.* **275**, 257 (1994).]

[83] L. Ukeiley, L. Cordier, R. Manceau, J. Delville, M. Glauser, and J. P. Bonnet, "Examination of large-scale structures in a turbulent plane mixing layer. Part 2. Dynamical systems model," J. Fluid Mech. **441**, 67 (2001).

[84] M. Couplet, P. Sagaut, and C. Basdevant, "Intermodal energy transfers in a proper orthogonal decomposition–Galerkin representation of a turbulent separated flow," J. Fluid Mech. **491**, 275 (2003).

[85] A. Glezer, Z. Kadioglu, and A. J. Pearlstein, "Development of an extended proper orthogonal decomposition and its application to a time periodically forced plane mixing layer," Phys. Fluids A **1**, 1363 (1989).

[86] G. Galletti, C. H. Bruneau, L. Zannetti, and A. Iollo, "Low-order modelling of laminar flow regimes past a confined square cylinder," J. Fluid Mech. **503**, 161 (2004).

[87] M. Bergmann, C.-H. Bruneau, and A. Iollo, "Enablers for robust POD models," J. Comput. Phys. **228**, 516 (2009).

[88] M. Pastoor, L. Henning, B. R. Noack, R. King, and G. Tadmor, "Feedback shear layer control for bluff body drag reduction," J. Fluid Mech. **608**, 161 (2008).